Bulletin of the Seismological Society of America. Vol. 59, No. 3, pp. 1365–1398. June, 1969

PRECISION OF EPICENTERS OBTAINED BY SMALL NUMBERS OF WORLD-WIDE STATIONS

By Jack F. Evernden

ABSTRACT

A fundamental error in the application of the confidence ellipse concept to the estimation of location error is demonstrated. The change in procedure required to be statistically sound and to achieve agreement with observations is explained and illustrated. The resultant procedure is then applied to the estimation of the network detection capability on a world-wide basis of the WWSSN.

Introduction

A pronounced contradiction between the predictions of probable error of determined epicenters and actual errors in epicenter locations can now be clearly illustrated. Table 1 illustrates this discrepancy between actuality and prediction when prediction is based upon confidence ellipse calculations as described in Flinn (1965). Table 2 presents computed location errors for numerous explosions when the network being used consisted of 4 stations well-distributed in azimuth and distance. Confidence ellipse calculations would have predicted 95 percent confidence ellipses with areas of 20,000 square kilometers when using observed data and approximately 4,000 square kilometers when using master-controlled data.*

The contradiction between prediction and actual location capability when using only a few detecting stations suggests strongly that the mode of prediction is in serious error and that epicenter locations as routinely done are much more accurate than has been generally believed. This paper will confirm the inadequacy of the presently employed confidence ellipse calculations and will indicate the necessary procedures required to accurately predict probable location errors (ignoring bias problems). As the 0.95 probability regions are shown to be quite small for even 4 to 6 station locations under certain assumptions of station distribution and standard deviation of travel-time data used, it becomes extremely important to enter the phase of refined seismological surveillance where regional travel-time curves are developed and the critical nature of station distribution is fully realized and exploited.

To begin with, it will be demonstrated on an empirical basis that the confidence areas predicted by standard procedures say little or nothing about the probable error of a computed epicenter location. It should be pointed out at the beginning of this discussion that the confidence ellipses as now computed are the so-called fiducial confidence ellipses. The only condition that these ellipses are intended to fulfill is that at, say, a 95 per cent confidence level, "95 per cent confidence ellipses" of 95 of 100 events will cover the mean epicenter. This definition says absolutely nothing about the relation between the area of a given fiducial confidence ellipse and probable location error. This statistical condition is both quantitatively and qualitatively markedly different than the condition for the ellipse which surrounds the true epicenter and includes 95 of 100 of the computed epicenters (assuming in both ellipses that errors in travel times

* The master event technique is to use the data from large events to evaluate the effect of earth inhomogeneities on P travel times (i.e., determine station residuals) and to then adjust the observed travel times for small events to create, for computational purposes, a fictional homogeneous Earth to which our travel-time curves apply in detail. See Evernden (1969) for an application of this technique.

TABLE I

Location of NTS Events by use of $P_g(t - \triangle/6.00)$

Event	Actual Location and Origin Time				Computations Based on Pg								δ † etc.		
	m'_b	Lat	Long	Origin	Stations	Quads	Lat	Long	Origin	S/MA*	S/MI*	Az*	Lat	Long	Origin
Bilby	5.6	37.06° N	116.02° W	17:00:00.1	4	4	37.05° N	116.05° W	17:00:00.5	37 km	31 km	69	1 km	−3 km	−00.4 sec
					14	4	37.07	116.01	17:00:00.0	17	11	56	−1	1	00.1
Aardvark	4.6	37.07	116.03	19:00:00.1	5	3	36.84	116.13	19:00:00.3	179	86	54	23	−10	−00.2
					13	4	37.12	116.00	19:00:00.1	21	15	40	−5	3	00.0
Hardhat	4.2	37.23	116.06	18:00:00.1	4	4	37.20	116.13	18:00:00.1	50	42	68	3	−7	00.0
					24	4	37.20	116.08	18:00:00.3	7	5	70	3	−2	−00.2
Cimarron	4.0	37.13	116.05	18:00:00.2	4	4	37.05	116.07	18:00:00.9	106	77	74	8	−2	−00.7
					22	4	37.13	116.06	18:00:00.6	11	7	76	0	−1	−00.4
Dorprime	3.7	37.04	116.02	18:00:00.1	4	3	37.05	116.06	17:59:59.1	500	216	67	−1	−4	01.0
					21	4	37.06	116.05	18:00:00.2	17	10	67	−2	−3	−00.1
York	3.7	37.12	116.04	15:00:00.2	4	4	37.17	116.07	15:00:00.4	191	112	73	−5	−3	−00.2
					11	4	37.15	116.08	15:00:00.4	7	6	54	−3	−4	−00.2
Dormouse	3.6	37.05	116.04	18:00:00.1	4	4	37.06	115.98	18:00:00.9	285	149	74	−1	6	−00.8
					24	4	37.08	116.00	18:00:01.2	19	12	65	−3	4	−01.1
Armadillo	3.5	37.04	116.04	16:30:00.1	4	4	36.95	116.09	16:30:02.1	82	67	71	9	−5	−02.0
					23	4	37.06	116.05	16:30:00.8	9	6	70	−2	−1	−00.7
Stillwater	3.5	37.13	116.05	18:00:00.2	4	4	37.14	116.03	18 00:01.6	6	5	70	−1	2	−01.4
					24	4	37.14	116.04	18:00:01.2	7	5	69	−1	1	−01.0
Wichita	3.5	37.13	116.06	21:00:00.2	4	4	37.08	116.19	21:00:01.5	120	69	73	5	−13	−01.3
					11	4	37.10	116.07	21:00:00.9	14	12	54	3	−1	−00.7
Bobac	3.4	37.05	116.02	17:00:00.1	4	4	37.15	116.03	17:00:01.0	227	133	73	−10	−1	−00.9
					11	4	37.12	116.08	17:00:00.6	7	6	39	−7	−6	−00.5
Chinchilla	3.2	37.05	116.03	16:30:00.1	4	4	37.04	116.10	16:30:01.5	274	226	70	1	−7	−01.4
					20	4	37.08	116.04	16:30:00.8	11	8	73	−3	−1	−00.7
Danny Boy	3.1	37.11	116.37	18:15:00.1	4	3	37.17	116.55	18:15:02.8	725	423	72	−6	−18	−02.7
					13	4	37.16	116.39	18:15:01.2	20	13	76	−5	−2	−01.1
Codsaw	3.1	37.13	116.04	17:50:00.2	4	4	37.18	116.07	17:50:01.9	80	67	69	−5	−3	−01.7
					20	4	37.14	116.03	17:50:01.4	7	5	73	−1	1	−01.2

* 95% Confidence Precision Ellipse. S/MA = Semi-major axis, S/MI = Semi-minor axis.

† $\text{Lat}_{\text{actual}}$ minus $\text{Lat}_{\text{computed}}$, etc.

are normally distributed at a given standard deviation). This distinction between fiducial confidence ellipses and probable error estimate is stressed strongly in all textbooks on statistics. The conclusion that will emerge from the discussions below is that our present procedures for estimating probable errors in epicenter locations suffer severely from this confusion of definitions and from the assumption that the fiducial confidence ellipses were approximate measure of probable location error. The procedure followed to demonstrate these facts is as follows (remembering that, when computing fiducial confidence ellipses, the assumption is made that travel-time errors are normally distributed):

TABLE 2

LOCATION ERRORS ASSOCIATED WITH VARIOUS NETWORKS

A

Event Location	Explosions: Nature of Network (4- station-Teleseismic-D=O) Network A	Network B	Network C	Average
Site A (9 events)				
Observed travel times	11–13 km	15–18 km	9–11 km	13 km
Master-controlled travel times	0–2	2–4	2–6	2½
Site B				
Observed travel times	24	26		25
Site C				
Observed travel times	8	9	11	9
Master-controlled travel times	—	4	8	6
Site D (14 Events)				
Observed Travel times		7 (2–10) km		
	Earthquakes (4-station—Teleseismic-pP)			
Site E (14 Events)				
Observed travel times		12 (5–22) km		
Master-controlled travel times		8 (1–16) km		

(a) Select one or more station networks and an assumed epicenter, the exact location of the epicenter being of no significance, though its general position relative to the network is critical.

(b) Compute travel times to all stations from the assumed focus according to a given travel-time curve. The travel-time curve used is immaterial, though it should be a near approximation to that appropriate to the Earth simply to maintain a sense of relevance in the exercise.

(c) Randomize the computed travel times according to a set of normally distributed random numbers with an assigned standard deviation. The value of standard deviation used depends upon assumptions relative to the quality of the travel-time curve and of the individual observations. An intensive study of Kamchatka/Kuril travel-time data indicates that:

(1) A standard deviation of 0.1–0.2 seconds is appropriate for master-controled data from high performance stations.

(2) A standard deviation of 0.5–0.6 seconds is appropriate for observational data from high performance stations relative to the travel-time curve of Herrin *et al* (1968)

(3) A standard deviation of 0.8—1.0 seconds is appropriate for observational data from WWSS stations relative to the HERRIN travel-time curve.

(d) Compute epicenter locations with the randomized data and determine the pattern of errors of location.

(e) Analyze the computed location by standard regression analysis (SRA) to determine pattern of location error.

Statistics

The procedure for estimating size, shape and orientation of the region of probable location error is to compute numerous test events such as have been described above and to then treat these sets of computed epicenters by normal bivariate statistical analysis. We assume that the possible errors in location of latitude and longitude have a continuous normal bivariate distribution. Assume first that the variable x (longitude) is normally distributed with standard deviation σ_1. Then if the variable is measured from its mean, the probability that the random value of x will fall in the interval dx is

$$dP_1 = \frac{dx}{\sigma_1 \sqrt{2\pi}} \exp\left(-x^2/2\sigma_1^2\right). \tag{1}$$

Assume next that the regression of y (latitude) on x is linear and homoscedastic. Then if σ_2 is the standard deviation of y in the distribution, the common variance of the arrays of y's is $\sigma_2^2(1 - \rho^2)$, where ρ is the coefficient of correlation between the variables. Finally, assume that each array of y's is normally distributed. Then, since the mean of each area is on the line of regression

$$y = \rho \times \sigma_2/\sigma_1, \tag{2}$$

and the variance of each array is as stated, the probability that a value of y, taken at random in an assigned vertical array, will fall in the interval dy is

$$dP_2 = \frac{dy}{\sigma_2 \sqrt{2\pi(1 - \rho^2)}} \exp\left[-\frac{1}{2\sigma_2^2(1 - \rho^2)}\left(y - \frac{\rho x \sigma_2}{\sigma_1}\right)^2\right]. \tag{3}$$

By the theorem of compound probability, the chance of a pair of variables (x, y) falling in the elementary rectangle $dx\,dy$ is

$$dP_1 dP_2 = \frac{dx\,dy}{2\pi\sigma_1\sigma_2 \sqrt{1 - \rho^2}} \exp\left[-\frac{1}{2(1 - \rho^2)}\left\{\frac{x^2}{\sigma_1^2} - \frac{2\rho xy}{\sigma_1\sigma_2} + \frac{y^2}{\sigma_2^2}\right\}\right]. \tag{4}$$

The probability density (x, y) for the distribution is therefore

$$\varphi(x, y) = \frac{1}{2\pi\sigma_1\sigma_2 \sqrt{1 - \rho^2}} \exp\left[-\frac{1}{2(1 - \rho^2)}\left\{\frac{x^2}{\sigma_1^2} - \frac{2\rho xy}{\sigma_1\sigma_2} + \frac{y^2}{\sigma_2^2}\right\}\right]. \tag{5}$$

Such a distribution is called a bivariate normal distribution and the variables are said to be normally correlated. The $z = \varphi(x, y)$ is the normal correlation surface. Since equation 8 is of the same form in x and in y, we may conclude that the regression of x on y is also linear.

The curves along which the probability density (or the relevant frequency density) is constant are the homothetic ellipses

$$\frac{x^2}{\sigma_1^2} - \frac{2\rho xy}{\sigma_1\sigma_2} + \frac{y^2}{\sigma_2^2} = \gamma^2. \tag{6}$$

If ξ and η are new rectangular coordinates obtained by rotation of the x, y axes through an angle θ such that

$$\xi = x\cos\theta + y\sin\theta, \qquad \eta = y\cos\theta = x\sin\theta, \tag{7}$$

the angle of rotation required in order to convert the ellipses of equation 6 into the form

$$\frac{\xi^2}{\sigma_\xi^2} + \frac{\eta^2}{\sigma_\eta^2} = \lambda^2 \tag{8}$$

is

$$\theta = \frac{1}{2}\tan^{-1}\frac{2\rho\sigma_1\sigma_2}{\sigma_1^2 - \sigma_2^2}. \tag{9}$$

With this change in variable, the exponential term in the expression for the probability density function of $\varphi(\epsilon, \eta)$ will take the form

$$\exp\left[-\frac{1}{2}\left\{\frac{\xi^2}{\sigma_\xi^2} + \frac{\eta^2}{\sigma_\eta^2}\right\}\right]. \tag{10}$$

The ellipses required for our purposes are those with a designated probability that a test epicenter is within them. Thus, we need to integrate $\varphi(x, y)$ over areas defined by the ellipses of the exponential coefficient. Thus, we want to integrate over an area Λ defined by the ellipse of equation 6 where $\rho = \mu_{xy}/\sigma_2\sigma_1$ and μ_{xy} is the covariance of x and y. What we wish to determine from this integration is the value of λ of equation 6 to be associated with an assigned value of probability P. By rotation of axes and change of variables in the integration, it can be shown that

$$\text{Probability } P = \iint \varphi(x, y, \lambda)\, dx\, dy = 1 - e^{-\lambda^2}. \tag{11}$$

Semi-axes equal $\lambda\sigma_\xi\sqrt{2}$ and $\lambda\sigma_\eta\sqrt{2}$, where $\sigma_\xi\sigma_\eta = \sigma_1\sigma_2\sqrt{1-\rho^2}$ and $\sigma_\xi^2 + \sigma_\eta^2 = \sigma_1^2 + \sigma_2^2$. Area of the λ-value ellipse is

$$A_\lambda = \iint_{\Lambda_\lambda} dx\, dy = 2\sigma_\xi\sigma_\eta\pi\lambda^2. \tag{12}$$

Since these ellipses are computed by regression analysis based on simulated epicenter runs, we have chosen to designate them as SRA ellipses in order to clearly differentiate them from any other types of computed probable error ellipses. On all figures of this report showing plots of epicenters, the ellipses presented are the 95 percent

SRA ellipses. It can be noted on several of the figures that the pattern of test epicenters does not appear to be actually obeying an elliptical distribution. This is not at all surprising from seismological considerations.

Several such investigations are presented in the figures of this report, all illustrating the same general result. Most figures present the result of running 100 test events for a particular station network and standard deviation of travel-time data. Each figure indicates the assumed position of the essentially randomly-placed stations relative to the assumed epicenter. The ring is placed at an epicentral distance of 70°.

The standard error figures given in column 4 of Table 3 are the computed "standard errors of single observation," i.e.,

$$(\sum (t_i - t_0)^2/N - 4)^{1/2}$$

where t_i is observed travel time, t_0 is computed travel time and N is number of stations used. Figure 3, derived from the data of Table 3, illustrates that there is no correlation between the computed "standard error of single observation" for each run and the computed shift in epicenter resulting from random alteration of the travel times. The computed standard error of single observation is the parameter used in normal fiducial ellipse calculations to control ellipse size. It immediately follows that there is no correlation between actual errors in epicenter location and the area of the computed fiducial confidence ellipses. This conclusion is also true for the probability of being within a 500 square kilometer zone or a 200 square kilometer zone around the computed epicenter, though the magnitude of the error is less than for areas defined by the 0.95 probability condition.

Table 4 summarizes the data of several studied networks. The "computed area" data of Table 4 were obtained by averaging the computed 95 per cent confidence ellipse areas for the 100 runs of each set. The "observed area" data were obtained for networks of Figures 1, 10, and 16 and Table 3 by standard regression analysis procedures described above. It can be seen that the size of the computed 95 per cent fiducial confidence areas is a gross overestimate in nearly all cases of the error in epicenter location accuracy. The discrepancy between fiducial confidence ellipse area and actual epicenter location error is greater for the 5-station network than for the 9-station network.

Discussion

Several points appear clear. The first is that the computed "standard error of a single observation" for individual runs is not a relevant parameter in estimating probable location error and is no measure of the standard deviation of the data employed relative to the travel-time curve used. The second point is the fiducial confidence ellipses generally grossly overestimate location error for events located by a few stations.

On the other hand, it can be seen from the data of Table 3 that the distribution of computed epicenters has a statistical relationship controlled by the network and standard deviation used. Therefore, the significant statistical parameter of the travel-time data that is relevant in location error estimate calculations is the empirically determined standard deviation of the data for stations of the type being used in the surveillance network relative to the travel-time curve. In the simulated runs of this note, we consider the travel-time curve to be perfect and that all errors in travel times are random errors around that curve and are not regional or distance correlated (the same assumptions as used in the fiducial confidence ellipse computations). This num-

TABLE 3

NETWORK: 9-STATION TELESEISMIC, 4-QUADRANT STANDARD DEVIATION OF RANDOM ADJUSTMENT OF TRAVEL TIMES—0.8 SECONDS
All solutions restrained to 0 Depth

Epicenter Shift			Standard Error* sec.	Fiducial Confidence Ellipse (95 per cent)			
Total km	δ Long (+ E) km	δ Lat (+ N) km		S/MA km	S/MI km	Area km²	AzS/MA
6.3	6.1	−1.5	0.9	34	18	1892	N89°E
11.8	−9.2	−7.4	0.9	34	18	1899	
7.0	4.1	5.6	1.0	38	20	2424	
7.4	−2.6	−6.9	1.1	41	22	2744	
4.1	−1.8	3.7	1.1	39	21	2569	
1.5	1.4	0.5	1.0	39	21	2514	
1.7	1.3	−1.0	1.0	37	20	2267	
8.5	2.0	−8.2	1.0	37	19	2247	
12.0	−11.5	3.6	0.7	27	14	1230	
1.3	−1.1	−0.8	0.5	18	9	529	
7.6	−7.4	−1.8	0.8	30	16	1457	
4.3	−4.3	0.1	1.0	38	20	2398	
7.6	−7.6	−0.4	0.8	29	15	1393	
7.4	4.1	−6.2	0.7	25	13	999	
7.6	5.1	−5.6	0.8	29	15	1418	
13.2	5.5	12.0	0.7	27	14	1173	
5.0	0.9	4.9	0.7	27	14	1233	
4.4	−1.7	4.1	0.3	13	7	259	
8.2	3.1	7.5	0.6	22	12	784	
6.1	3.6	−4.9	0.7	28	15	1274	
9.0	8.9	−0.7	0.4	17	9	453	
16.2	−2.5	16.0	0.7	24	13	980	
1.0	−0.4	0.9	0.9	32	17	1736	
4.5	2.1	−3.9	0.5	20	11	661	
9.1	−9.0	−1.5	1.2	45	23	3274	
4.6	4.5	1.1	0.7	28	15	1258	
3.8	−3.6	1.2	0.9	33	18	1847	
6.7	6.4	1.7	0.6	21	11	753	
8.1	−3.7	−7.2	0.3	9	5	147	
6.5	3.9	5.2	0.9	33	17	1764	
9.5	8.1	5.0	0.4	15	8	378	
4.4	4.0	−1.7	0.8	30	16	1497	
4.6	−1.3	−4.4	0.8	29	15	1351	
4.4	−2.5	3.5	0.6	24	13	927	
1.5	1.0	−1.2	1.3	49	26	3926	
4.0	3.7	1.6	1.0	38	20	2373	
3.5	0.8	−3.4	0.7	27	14	1207	
7.5	−7.5	−0.7	0.6	21	11	719	N89°E
7.3	7.3	0.2	0.7	27	14	1173	
2.9	1.7	−2.3	0.9	32	17	1667	
8.2	7.5	−3.2	1.0	37	20	2280	
3.8	−3.8	−0.3	0.6	22	12	805	
12.8	−0.8	12.8	0.8	30	16	1499	
5.3	1.1	−5.2	0.6	23	12	891	
8.7	−5.7	6.6	1.0	36	19	2131	
3.8	1.4	−3.5	0.5	17	9	501	
5.7	5.3	2.2	0.6	23	12	905	
4.8	−4.8	0.2	0.8	29	15	1355	
8.6	5.4	6.8	1.4	52	27	4394	

TABLE 3—*Continued*

Epicenter Shift			Standard Error* sec.	Fiducial Confidence Ellipse (95 per cent)			
Total km	δ Long (+ E) km	δ Lat (+ N) km		S/MA km	S/MI km	Area km²	AzS/MA
8.7	−7.6	4.4	0.6	24	12	911	
10.8	−10.1	3.9	1.0	35	19	2068	
2.6	0.2	−2.6	0.7	24	13	986	
10.2	−4.4	−9.2	0.9	33	17	1775	
6.0	−0.6	6.0	0.6	23	12	877	
9.3	−3.2	8.8	1.0	36	19	2147	
9.4	−8.5	−4.1	0.7	28	15	1263	
4.2	−3.3	2.7	0.8	29	16	1434	
7.5	−6.5	−3.8	0.7	25	13	1034	
5.4	4.2	3.5	0.7	25	13	1038	
8.8	−8.6	1.8	0.6	24	13	936	
10.4	−0.9	−10.3	0.9	35	18	1995	
12.2	6.6	10.2	0.6	23	12	886	
5.0	−1.0	−4.9	0.9	32	17	1668	
5.9	0.6	−5.9	0.7	26	14	1154	
5.2	3.7	−3.7	0.7	27	14	1175	
7.1	−6.8	−2.2	1.2	43	23	3119	
0.6	0.6	−0.1	0.7	27	15	1247	
7.2	5.8	4.3	0.6	22	12	826	
6.1	−5.7	2.0	0.7	25	13	1001	
6.0	−2.6	5.4	1.0	36	19	2110	
8.8	−8.5	−2.3	1.1	42	22	2916	
10.7	−8.6	6.3	0.3	12	6	225	
4.4	−2.7	−3.5	1.2	46	24	3540	
2.7	−2.7	0.4	0.7	24	13	977	
4.0	−3.1	2.5	0.3	12	6	229	
2.2	−1.8	1.3	0.6	22	12	814	
3.0	0.5	−2.9	0.9	32	17	1691	
5.3	−1.4	5.1	1.3	49	26	3971	
7.3	4.7	−5.6	1.2	43	23	3057	
4.2	0.3	−4.2	0.8	29	15	1372	N89°E
17.0	16.7	−3.2	0.7	25	13	1060	
6.9	5.4	−4.3	0.7	26	14	1113	
3.9	−3.0	−2.5	1.0	38	20	2357	
3.9	3.3	−1.9	0.7	25	13	1034	
10.1	6.8	7.4	0.8	30	16	1502	
2.4	2.2	−0.9	0.9	35	18	2009	
7.4	−7.1	2.1	0.9	33	18	1830	
7.1	0.8	7.1	0.7	27	14	1171	
11.4	11.4	0.3	0.9	34	18	1865	
3.0	−0.2	3.0	0.8	30	16	1443	
4.9	1.9	4.6	1.2	45	24	3392	
6.2	−5.9	−2.0	1.1	40	21	2623	
11.9	11.9	1.1	0.6	22	12	812	
10.9	−10.0	−4.3	1.1	39	21	2527	
7.5	7.3	−1.6	0.7	27	14	1182	
7.6	6.6	3.8	0.9	32	17	1715	
8.1	7.7	−2.7	0.5	17	9	498	
3.6	−1.1	−3.4	1.0	38	20	2404	
9.3	9.3	0.6	0.9	32	17	1703	
6.0	−4.9	3.4	1.0	36	19	2189	
Average	.05	.14		30	16	1584	

* Standard error of a single observation.

Standard deviation of single longitude shift values = 5.5 kilometers.

Standard deviation of single latitude shift values = 4.9 kilometers.

Area including 95% of computed epicenter = 338 square kilometers.

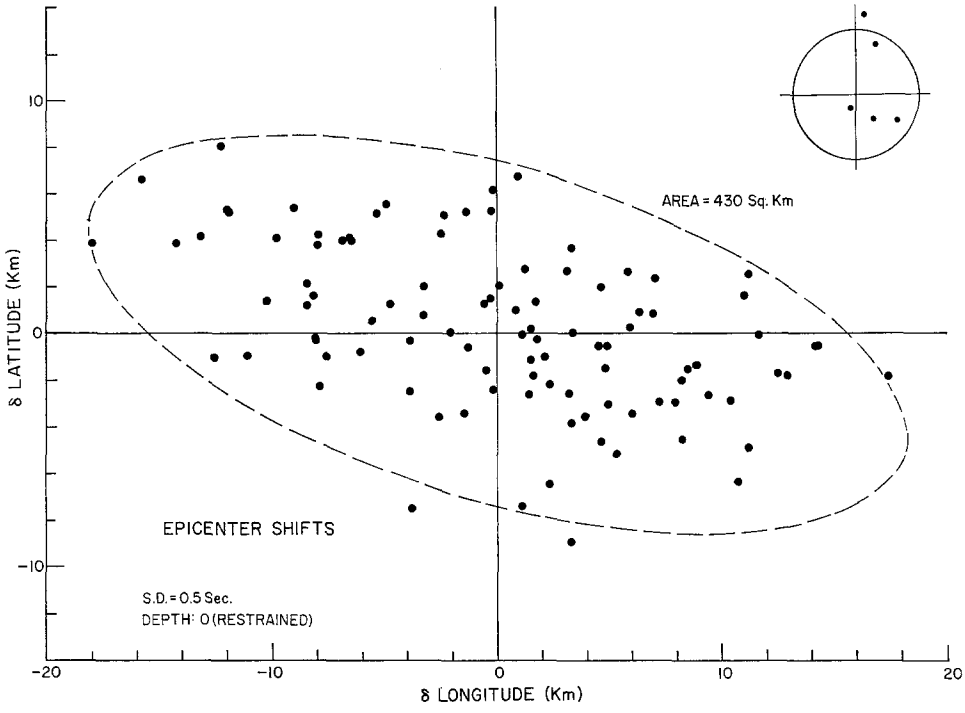

FIG. 1. Epicenter shifts.

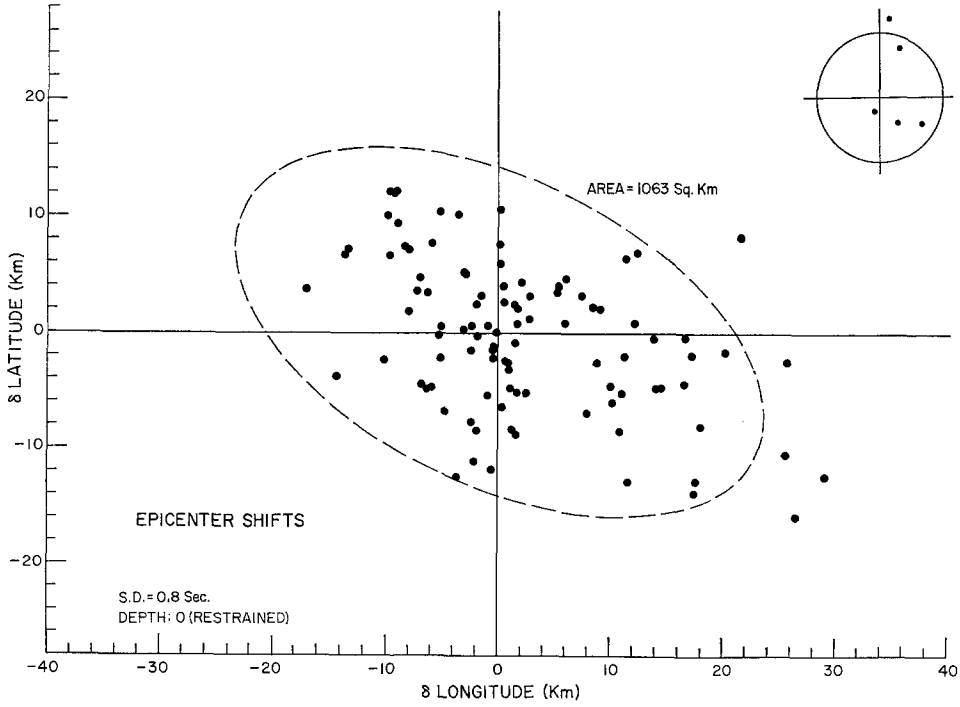

FIG. 2. Epicenter shifts.

ber is not determinable from the data of a few stations for a given event, as evidenced by the variation of the computed "standard errors of a single observation" from 0.2–1.4 seconds for the set of runs of Figure 3, where the actual standard deviation of the random data used was 0.8 seconds. The standard deviation of the travel-time data

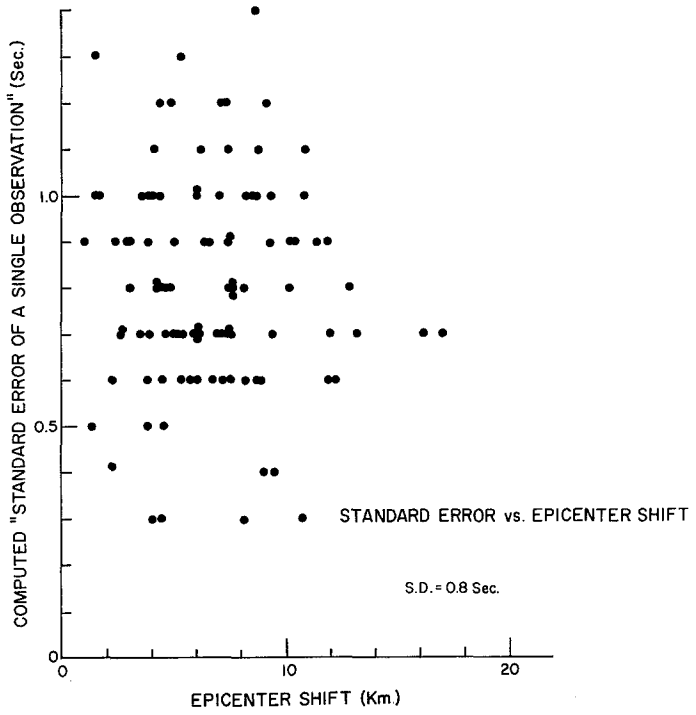

FIG. 3. Epicenter shifts.

TABLE 4

OBSERVED AREAS VERSUS COMPUTED AREAS

Network	S.D.	Restraint	Observed Area	Computed Area
			95% SRA Ellipses Area (km²)	95% Mean Fiducial Confidence Ellipses Area (km²)
Figure 1	0.5	(D = 0)	430	4490
	0.8	(D = 0)	1060	11240
Table 3	0.5	(D = 0)	200	650
	0.8	(D = 0)	510	1580
Figure 10	0.2	No	222	750
	0.5	No	990	3760
Figure 16	0.2	No	50	310
	0.5	No	490	2210

must be estimated,either as the standard deviation of the travel-time data for many events located by a few stations (the average computed error of single observation for the 100 runs of Table 3 is 0.79 seconds, i.e., essentially identical to the standard deviation of the random numbers used) or as the standard deviation of the travel-time data for an event located by many stations. The distribution of computed errors in location are controlled by this number rather than by the individual event values of com-

puted standard deviation for events located by a few stations. It should be noted, however, that use of this mean standard number in the regular fiducial confidence ellipse calculations does not remedy the problem of computing fiducial confidence ellipses greatly exceeding probable location errors.

A further interesting point is to be seen by considering the data of a few additional sets of events (Figures 1, 2, 6, 7, 8, 9, 10, 11 and Table 3). All test events discussed to this point in the report were run with depth restrained to the surface. Table 5 presents a summary of the 0.95 probability areas for these several networks. The data of Table 5 seem to clearly support several conclusions. The most critical point is that the 95 per cent SRA ellipses for 4-station locations with an optimum azimuthal distribution of stations (i.e., 4-quadrant) can be very small when using observed data having a standard deviation = 0.5 seconds, and SRA ellipses cover less than 100 square kilometers for

TABLE 5

EMPIRICAL DETERMINATION OF AREA OF 95 PER CENT CONFIDENCE REGIONS

Network	Standard Deviation of Randomized Data		
	0.2	0.5	0.8
4-Station Opposite Quadrant (See Figures 8, 9)	120 square km	580 square km	1300 square km
4-Station 3-Quadrant (See Figures 6, 7)	100	560	1300
4-Station 4-Quadrant (See Figures 4, 5)	70	320	750
5-Station 3-Quadrant (See Figures 1, 2)	—	430	1060
9-Station 4-Quadrant (See Table 3)	15	210	510

4-station locations with at least opposite quadrant distribution of stations when using master-controlled data. Thus, rather than having an unbelievable appearance of accuracy, the location errors presented in Table 2 for 4-station locations of explosions are indicated to be consistent with theoretical expectations and this empirical study. Note also from Table 5 that the data obtained support the intuitive conclusion that 3-quadrant distribution of stations is superior to opposite quadrant distribution and 4-quadrant distribution is superior to either opposite quadrant or 3-quadrant control.

It is obvious that new procedures must be developed for estimating probable errors in location for events located by a few stations. One such procedure has been discussed in detail above. Before proceeding to a discussion of another approach, it should be pointed out that estimates of errors in location resulting from use of given networks does not require actual travel-time data. The estimates of error and epicenter location residing in a given network of stations can be determined by this technique independently of earthquake or explosion data from the region. Since the estimate of standard deviation of the data is being made by procedures independent of the events being located, the error calculations do not require data for specific events. Thus, without an intensive study of observed data from all over the World, it should be possible to estimate the location accuracy of any network for events occurring in any part of the World. Of course, the problem of location bias (i.e., mislocation of LONG SHOT by teleseismic data) is not addressed by any of these ellipse calculations. See below for an example of estimating the location capability of a world-wide seismographic network.

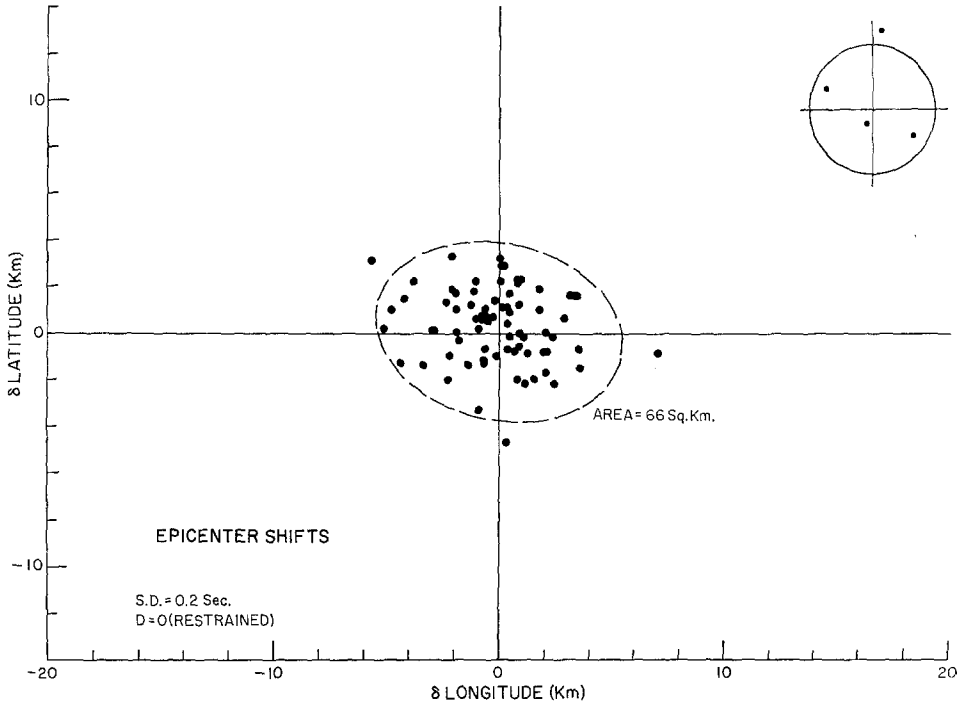

FIG. 4. Epicenter shifts.

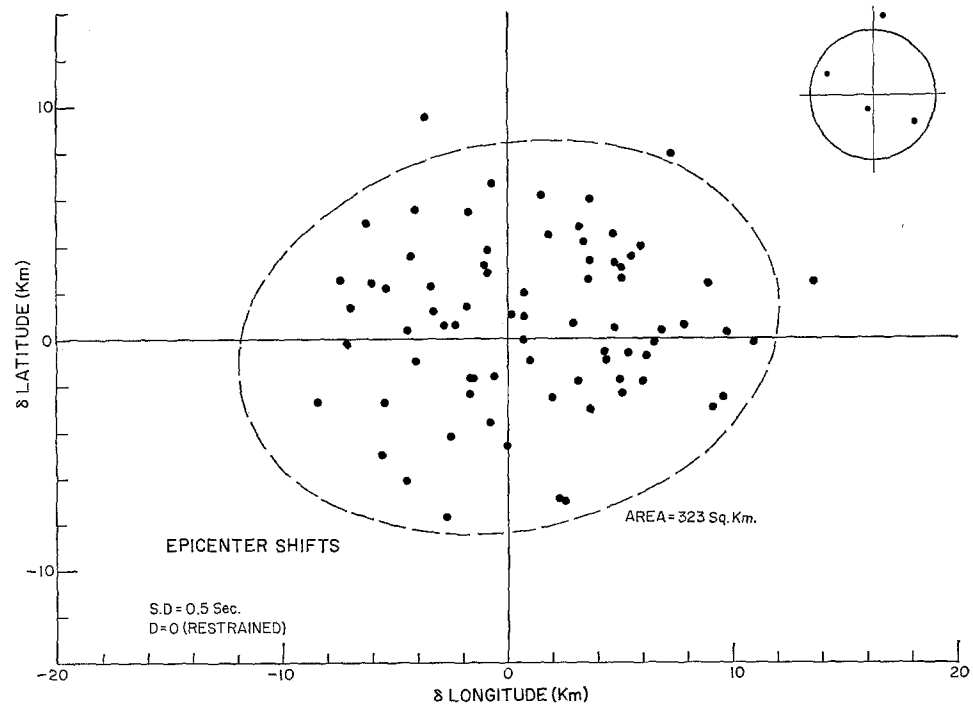

FIG. 5. Epicenter shifts.

The possible change in procedure to be discussed is to modify parameters used in the normal fiducial confidence ellipse calculations and, by so doing, to convert these from fiducial confidence ellipses into probable error of location ellipses. If the standard deviation of travel-time data can be assumed known from previously recorded data,

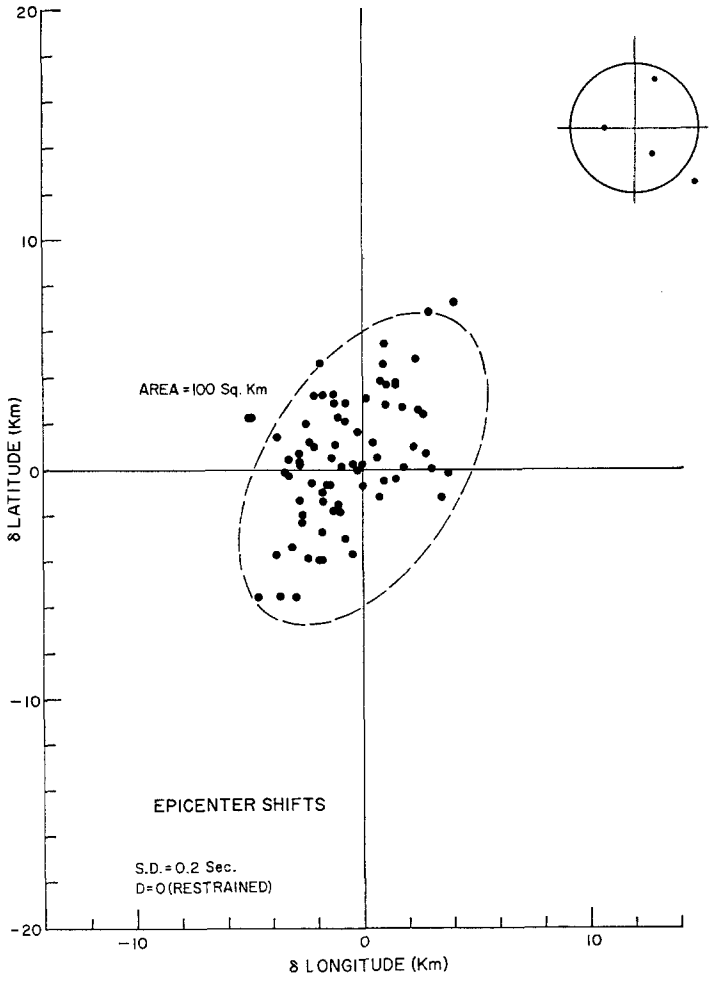

FIG. 6. Epicenter shifts.

the F statistic ($F_{2,N-4}$) used in the fiducial confidence ellipse calculations can be replaced by the χ_2^2 statistic with a pronounced reduction in predicted area of ellipse so achieved.

The normal epicenter location program computes a fiducial confidence ellipse for the coordinates of the location of, say,

$$z = (x, y)$$

when x and y are the correct latitude and longitude coordinates for the event. The technique assumes that the variances in the travel times, t_i, are unknown and must be

estimated from the data supplied for the location. The program generates an ellipse of the form

$$(\hat{\underline{z}} - \underline{z})' S_{11-2} (\hat{\underline{z}} - \underline{z}) = 2s^2 F_{2,N-4} = C^2 \tag{13}$$

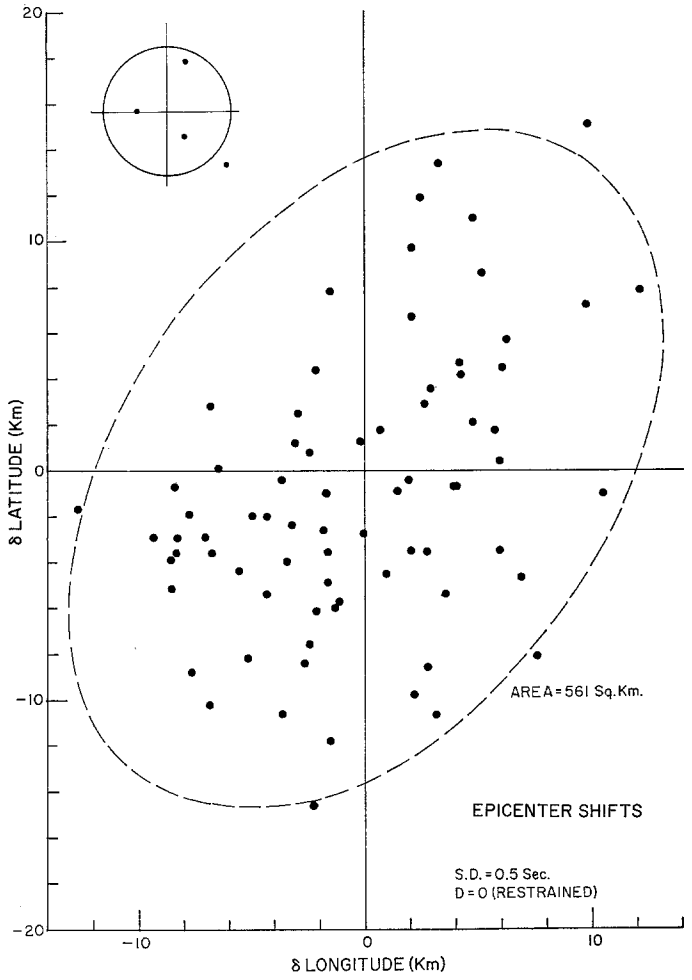

FIG. 7. Epicenter shifts.

where $\hat{\underline{z}} = (\hat{x}, \hat{y})$ are the estimated coordinates, s^2 is the estimated residual variance, S_{11-2} is the inverse of the 2×2 submatrix corresponding to x and y in the inverse of the normal equation matrix, and $F_{2,N-4}$ is an appropriate percentage point on the F distribution. Since the estimate of variance of t_i must be derived from the data supplied for the location, the extremely conservative F statistic must be employed. The resultant fiducial ellipse derives from the fact that x and y have a joint bivariate normal distribution with a variance-covariance matrix given by $\sigma^2 S_{11-2}^{-1}$. Hence, slices of constant probability generate two-dimensional ellipses. The proper interpretation of the ellipses is that 100 $(1 - \alpha)$ per cent of the ellipses generated should cover the true center. This is not at all the same thing as that ellipse surrounding the true epicenter which will

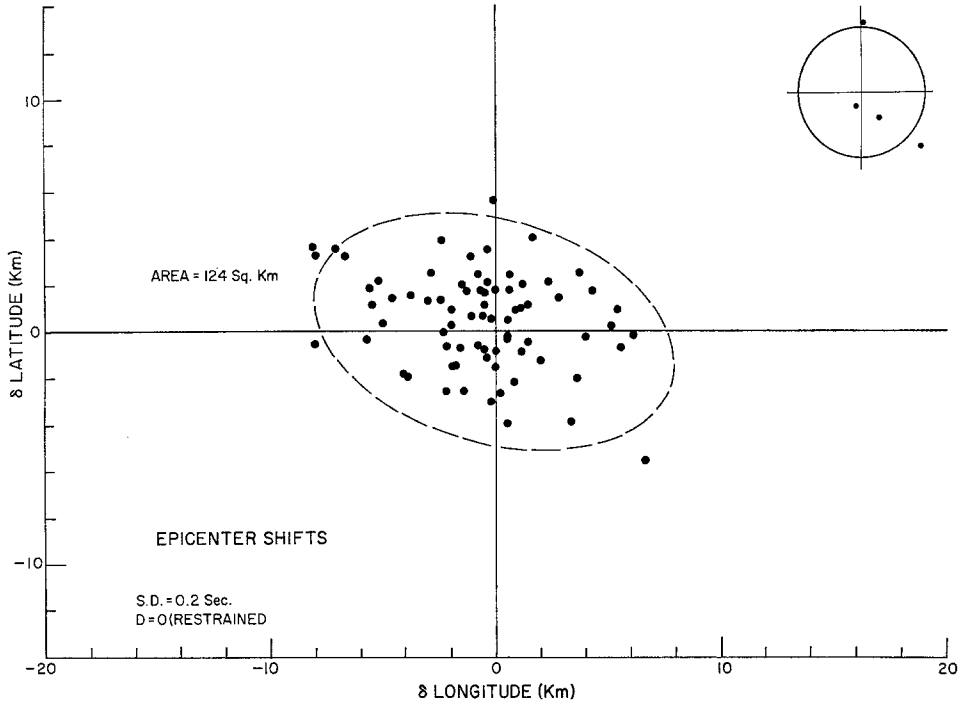

FIG. 8. Epicenter shifts.

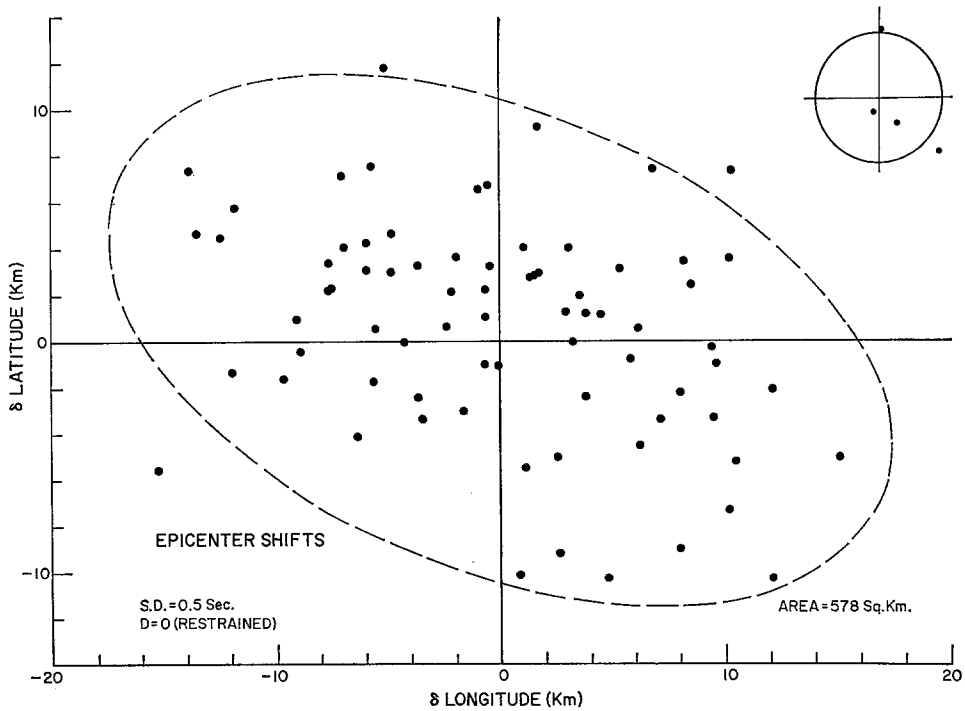

FIG. 9. Epicenter shifts.

cover 100 $(1 - \alpha)$ per cent of the computed epicenters deriving from t_i data of a given variance. That these are profoundly different concepts may be best illustrated by examples of which numerous have and will be presented. As a matter of fact, the fiducial ellipses computed in these empirical exercises do fulfill their proper condition (i.e., approximately 95 to 100 of the 95 per cent fiducial ellipses cover the mean epicenter) while yielding ellipse areas showing no relation to actual errors in epicenter locaton.

If we can assume that the variances of the travel times are a known constant σ^2, the confidence ellipses can be written

$$(\hat{\underline{z}} - \underline{z})' S_{11-2} (\hat{\underline{z}} - \underline{z}) = \sigma^2 \chi_2^2 = C'^2 \tag{14}$$

where χ_2^2 is an appropriate point (α) on the chi square distribution with 2 degrees of freedom. The constants C^2 and C'^2 of equations (13) and (14) respectively are related

TABLE 6

INDICATED RATIOS

	5 Stations		6 Stations		7 Stations		8 Stations		9 Stations	
$L_1'/L_1 = L_2'/L_2$	.75	.95	.75	.95	.75	.95	.75	.95	.75	.95
	.43	.12	.68	.40	.78	.56	.83	.66	.86	.72
A'A	.19	.02	.46	.16	.61	.31	.69	.43	.75	.52

to the lengths of the semi-axes of the ellipses by

$$\begin{aligned} L_1^2 &= C^2/a', \qquad L_2^2 = C^2/b' \\ L_1'^2 &= C'^2/a', \qquad L_2'^2 = C'^2/b' \end{aligned} \tag{15}$$

while the area of the ellipse determined by C^2 is $A = \pi L_1 L_2$ and the area determined by C'^2 is $A' = \pi L_1' L_2'$. Now, we can relate A_1', L_1', and L_2' to $A_1 L_1$, and L_2 by

$$\frac{L_1'}{L_1} = \frac{C'}{C}, \frac{L_2'}{L_2} = \frac{C'}{C}, \frac{A'}{A} = \frac{C'^2}{C^2}.$$

The following table gives the ratio of lengths and areas for the two conditions of assuming travel-time variance known and unknown, values being given for the probability levels of .75 and .95. We assume that s^2 in the normal (variance unknown) procedure is replaced by $Es^2 = \sigma^2$ when variance is assumed known. Table 6 then gives the indicated ratios. For example, with 5 stations, at a confidence level of 0.95, the axes of the A' ellipse (variance assumed known) are $\frac{1}{8}$ the length of those of the A ellipse (variance unknown) while A' is $\frac{1}{50}$ of A. Given the knowledge of the true variance, the ratio of ellipse dimensions can be found by

$$\frac{C'}{C} = \frac{\sigma}{s}\left(\frac{\chi_2^2}{2F_{2,N-4}}\right)^{1/2}$$

where s is the value that the normal program computes for the residual variances of a single observation from the data of the event being located. The values of A'/A for N station detection with one parameter restrained can be found from Table 6 by use of the column for $N + 1$ stations.

As discussed above, the normal earthquake location program can be used for simulation runs by computing exact travel times from a test epicenter to a given set of stations, applying normally distributed random errors of an assigned variance to these times, and then using the epicenter location program with these randomized times. In this case, for a constant σ^2 and fixed network of N stations, the estimates (x, y) have a joint normal distribution and arrange themselves in a probability pattern about the true epicenter. This pattern may be approximated by elliptical contours of constant probability. The predicted χ_2^2 values are introduced to replace the $F_{2,N-4}$ values, and σ^2 is inserted and used for ellipse calculations rather than the estimated residual deriving from the program.

The program then generates, in effect, the ellipse of equation (14) as a function of the estimated locations

$$\underline{z} = (x, y)$$

TABLE 7

SRA AND χ_2^2 ELLIPSE DIMENSIONS

Network	S.D.	Restrained Parameter	SRA		χ_2^2	
			Direction of Semi-Major Axes	Area of 95% SRA Ellipse	Direction of Semi-Major Axes	Area of 95% χ_2^2 Ellipses
	sec		*deg*	*km²*		*km²*
See Figure 1	0.5	D = O	N 75 W	430	N 76 W	439
See Figure 2	0.8	D = O	N 66 W	1063	N 76 W	1123
See Table 3	0.5	D = O	N 87 E	199	N 87 E	215
See Table 3	0.8	D = O	N 82 E	506	N 87 E	551
See Figure 10	0.2	None	N 31 W	222	N 30 W	180
See Figure 12	0.5	None	N 32 W	992	N 30 W	1144
See Figure 14	0.2	None	N 35 W	105	N 37 W	104
See Figure 16	0.5	None	N 40 W	486	N 37 W	651
See Figure 18	0.2	None	N 36 W	79	N 38 W	70
See Figure 20	0.5	None	N 39 W	402	N 38 W	438

rather than as a function of the true locations $z = (x, y)$. We are then computing ellipses which should describe the distribution of the randomized epicenters about the true epicenter, i.e., we are no longer computing fiducial ellipses but are computing that quantity of relevance in estimating the accuracy of computed epicenters.

As noted above, these new ellipses will have the identical orientation and eccentricity as those computed from the regular program but will be markedly smaller, particularly for station locations based on 4 to 8 stations. The result of these computations, with the previous ellipse program modified for assigned standard deviation of travel-time data and for use of the χ_2^2 statistic rather than the F statistic, can be compared with the SRA ellipses.

If the χ_2^2 ellipse calculations are compared with the SRA ellipse values, the data of Table 7 are obtained. In cases of no restrained parameters or restrained depth of focus, the predicted orientations, eccentricities and areas by the SRA and χ_2^2 techniques are nearly identical. The small differences probably arise as a result of the limited sample size used in the SRA calculations. This expected agreement of the two techniques means that a fast network program estimating worldwide location capability of a specified network is now possible by use of the modified χ_2^2 ellipse calculations.

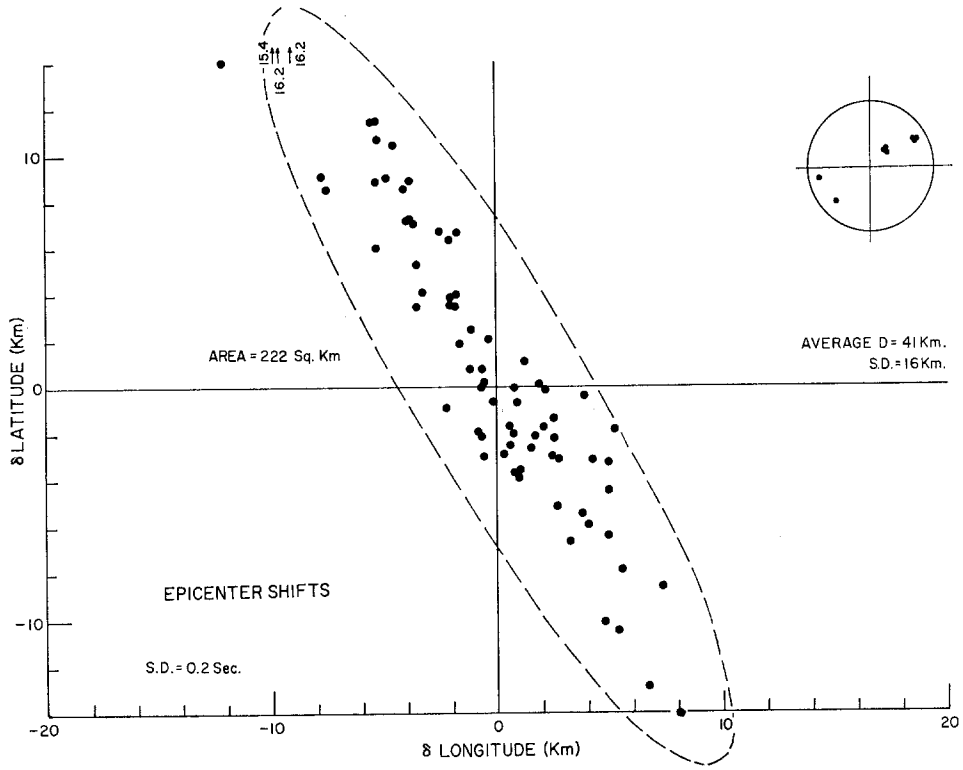

FIG. 10. Epicenter shifts.

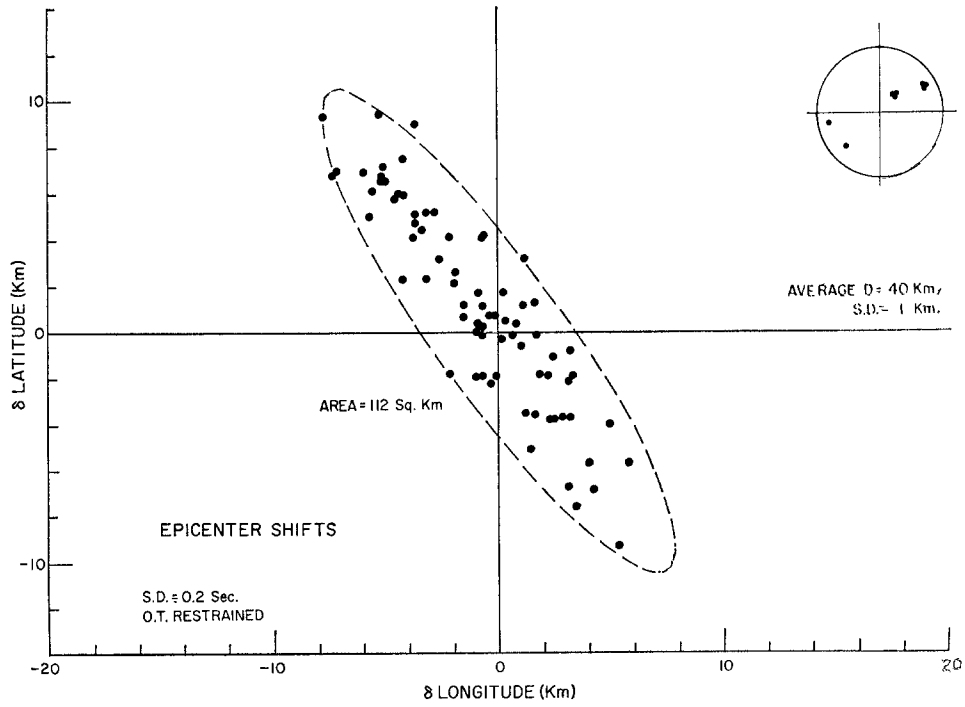

FIG. 11. Epicenter shifts.

With this technique of computing accurate χ_2^2 probable error or SRA ellipses now available, an investigation of different patterns of station distribution can be conducted. The location accuracy attainable with various additional networks is shown in Figures 10 through 23. Both data with s.d. of 0.2 seconds (master-controlled data) and 0.5 seconds were investigated with origin time both restrained and unrestrained, travel times having been computed for a 40-kilometer depth of focus. The basis for restraint

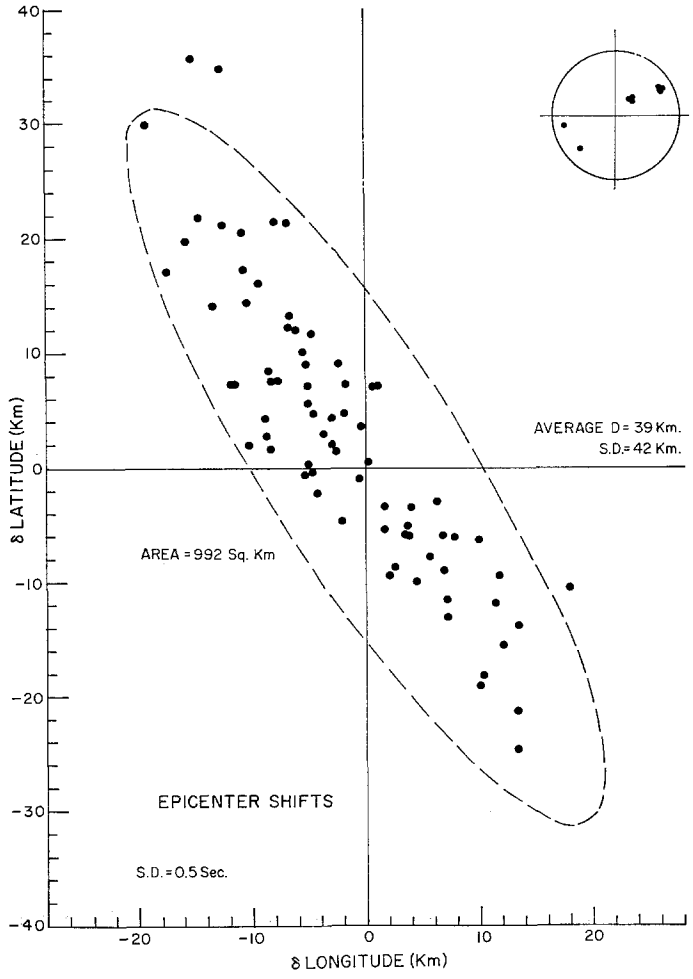

FIG. 12. Epicenter shifts.

of origin time is the demonstrated usefulness of S-P estimates of origin time in depth calculations. The significance of restraining the origin time as regards determining depth of focus has been detailed in a previous report. The high eccentricity of the SRA ellipses is clearly apparent on the figures, the restraining of origin time having a comparatively small effect on the size of these ellipses. However, it is seen either on the figures or in Table 6 that master-controlled data for a network as azimuthally poorly distributed as this still yields 95 per cent SRA ellipses with an area of only 220 square kilometers. With origin time restrained, the area of this ellipse decreased to 112 square kilometers. Note on Figures 10 and 11 that the most significant effect of restraining origin time was to improve the depth calculation. With master-controlled data and this

network, average depth of 75 test runs was 41 kilometers with s.d. of 16 kilometers, while if the origin time was restrained the average depth was 40 kilometers with s.d of 1 kilometer. The effect of this restraint of origin time is even more clearly shown on Figures 14 and 15 where observed (unadjusted) data were assumed. If origin time was not restrained, average depth was 39 kilometers with a s.d. of 42 kilometers, while, with origin time restrained, data of the same quality yielded an average depth of 40 kilo-

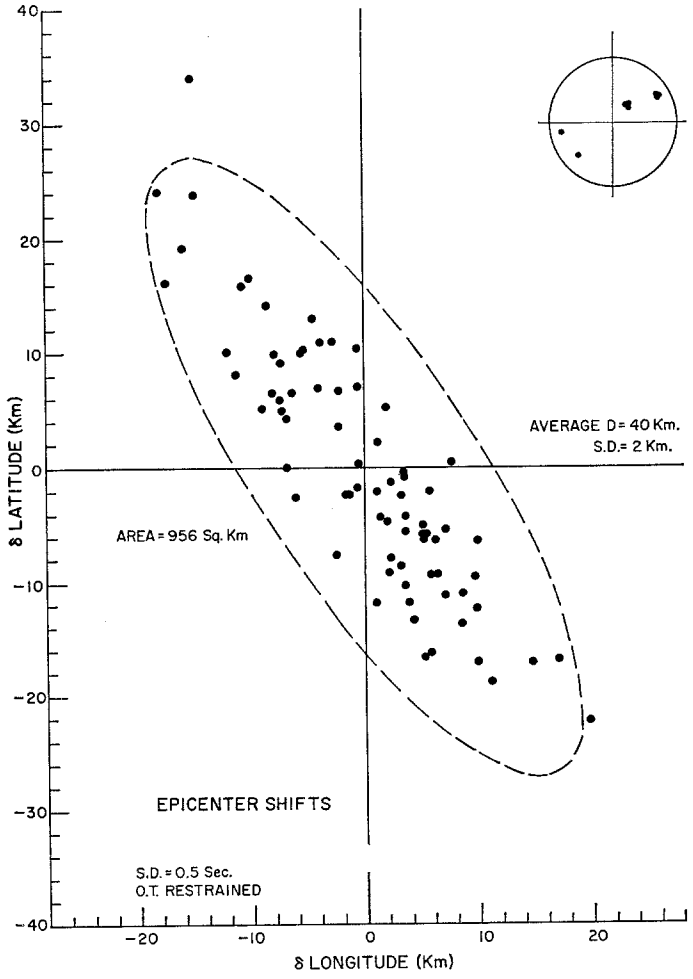

FIG. 13. Epicenter shifts.

meters with s.d. of 2 kilometers. The area of the 95 per cent SRA ellipses did not decrease particularly when origin time was or was not restrained.

The assumptions inherent in all ellpse calculations are that starts of phases are measurable to tenths of a second, the random errors around the mean travel-time curve being associated with slight timing errors and local structure and, thus, travel-time anomalies at the source and receivers, and that the travel-time curve used is statistically the correct curve so that residuals are not distance dependent. The size of the random component due to timing error and record quality depends upon the type of station being used. It is clear that the type of records obtained and the quality of timing used at Worldwide Standard Stations (WWSS) introduces a randomness in the data of

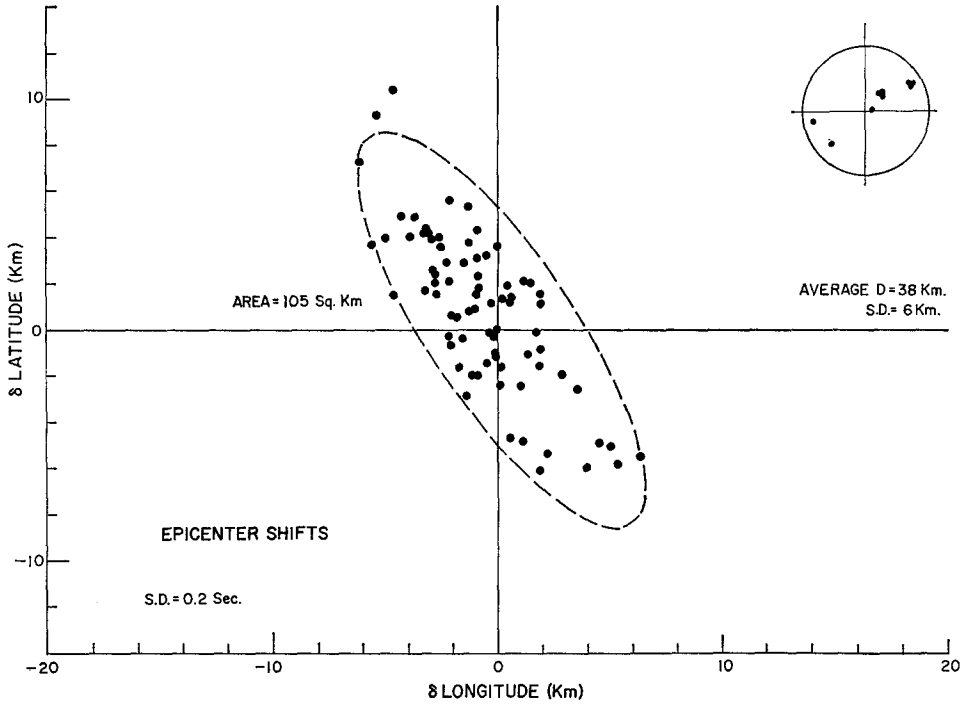

FIG. 14. Epicenter shifts.

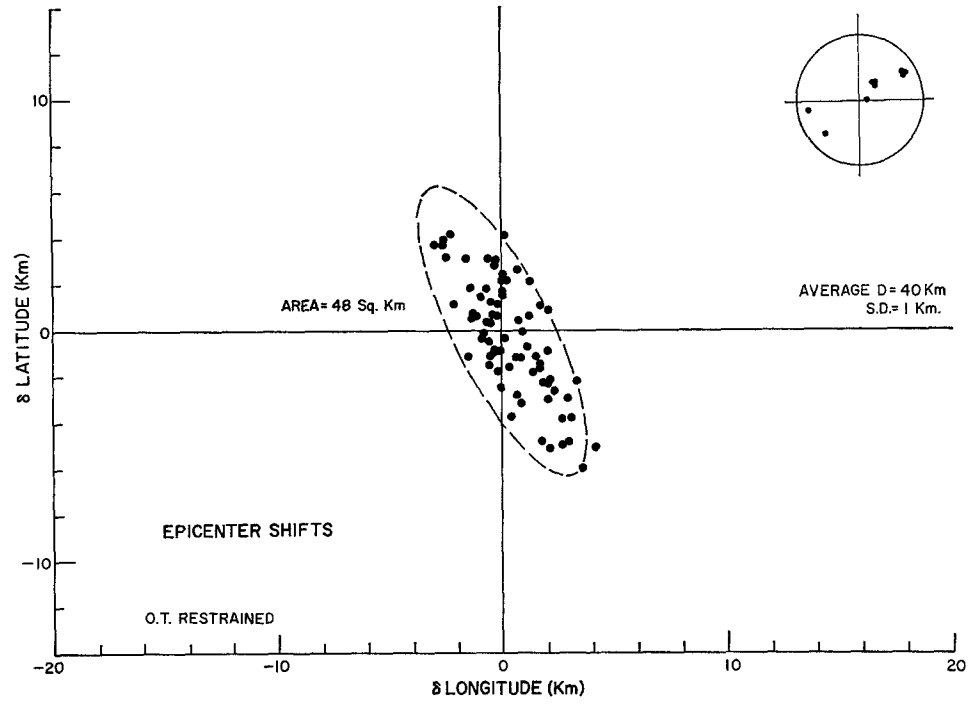

FIG. 15. Epicenter shifts.

more than 0.5 seconds. The elimination of dependence of observed residuals on distance certainly requires regional travel-time curves. Data now in hand and soon to be published indicate real and measurable variation in travel time as a function of location of the epicenter.

A subject requiring mention is the matter of travel-time bias. This term is intended to refer to local travel-time velocity structures which introduce travel-time anomalies

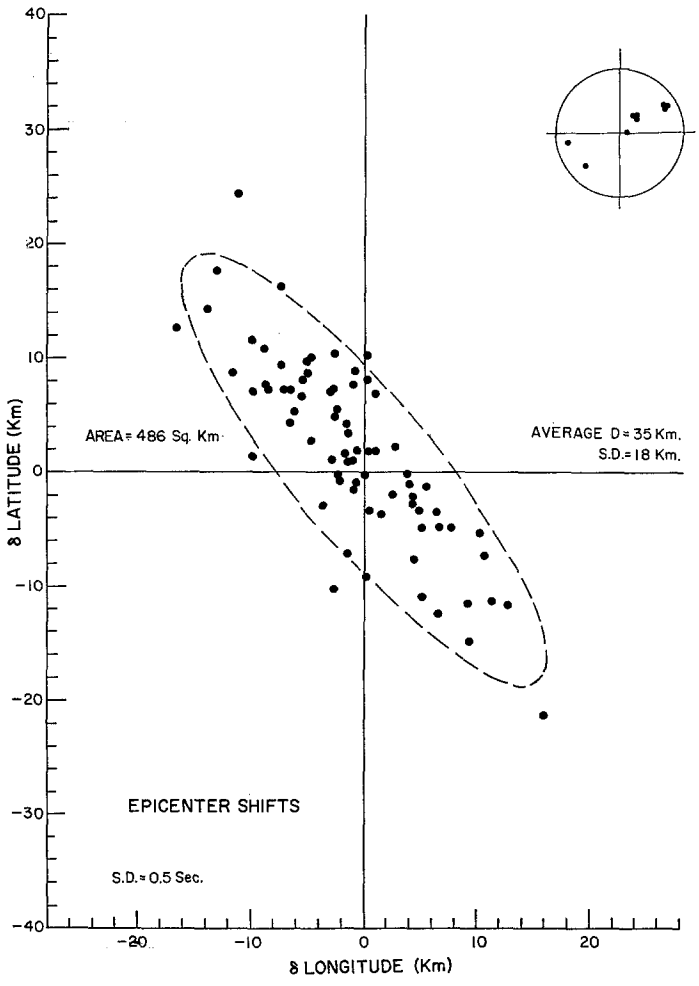

FIG. 16. Epicenter shifts.

such that travel times to the same distance in different directions are different. This is a distinctly different phenomenon than having an incorrect travel-time curve as a function of distance. These local bias factors can only be determined by local networks of seismologcal stations or by use of calibration explosions. Once determined, travel-time curves for a given area can be calibrated and the usefulness of the near stations then largely disappears. All events in hand today suggest that travel-time bias of this type is of small importance in continental areas, i.e., location errors of 8 kilometers or less are to be expected from this factor. Data reported by Gene Herrin (personal communication) indicate that, by correlation of computed epicenters and geological structure of Kamchatka Peninsula, travel-time bias in this area can be demonstrated to

introduce location errors of 6 kilometers or less. Data from the Kurile Ocean Bottom Seismemeter experiment indicate very little location bias present well off-shore. Data for LONGSHOT (Amchitka, Aleutian Islands) and for an Hawaiian earthquake (E. Herrin, personal communication) indicates that location bias may be 20 km or more in such regions.

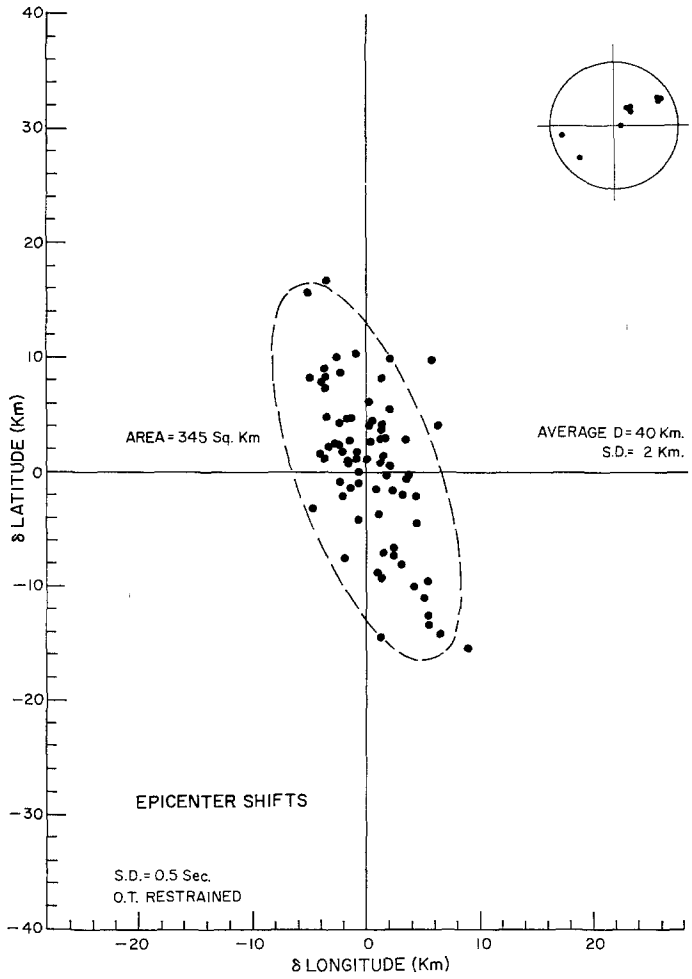

FIG. 17. Epicenter shifts.

A few further comments on the use of χ_2^2 ellipses rather than F ellipses may be useful. If it is felt that a completely unbiased estimate of probable location error is required, the F statistic or confidence ellipse may be used. However, this seems to the author to be an unwarranted degree of conservativism in use of available data. All of these discussions, both for confidence and coverage ellipses, assume accurate determination of phase beginnings on all records. Neither approach can pretend to take account of inaccurate observation of this quantity due to low signal-to-noise ratio. In general, such errors are not at all randomly distributed and are thus not interpretable by means of such ellipse calculations as here discussed. The only approach to recognizing such errors in travel times is inspection of the solutions to see whether unusually high station errors

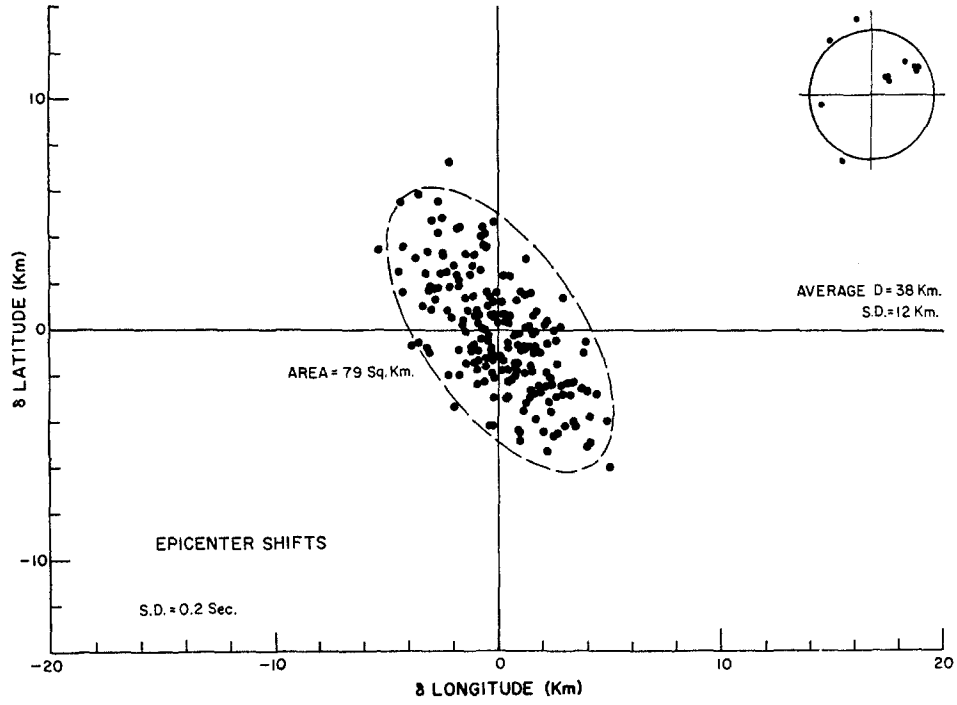

FIG. 18. Epicenter shifts.

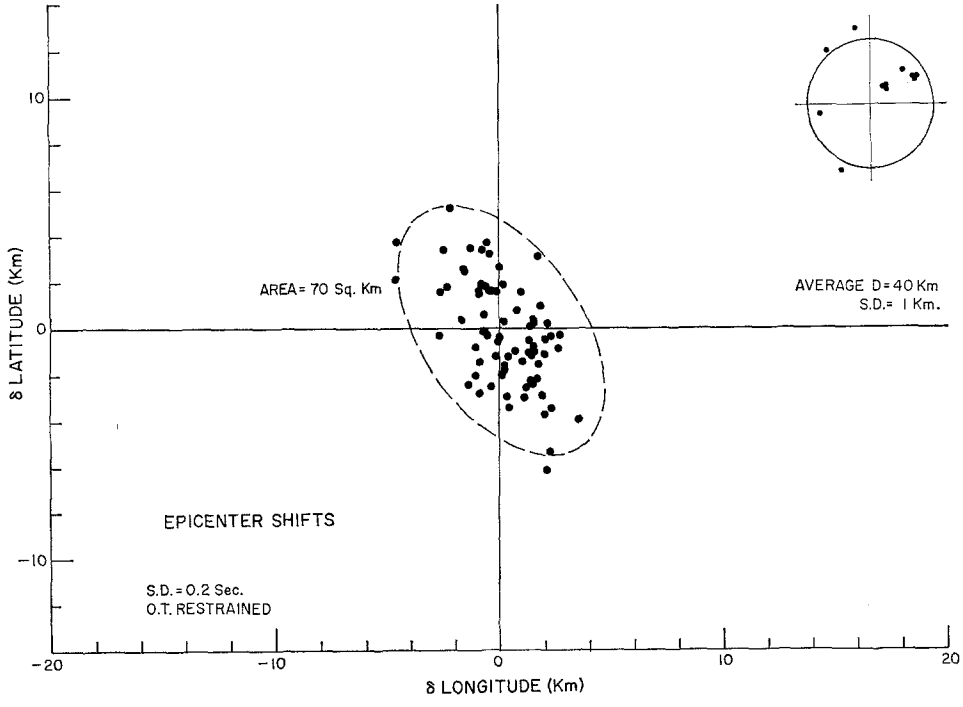

FIG. 19. Epicenter shifts.

are in the data. Therefore, under the assumption that phase beginnings were accurately determined, the use of χ_2^2 or coverage ellipses is justified and warranted if empirical analysis of the data of many events indicates that observed travel-time errors do obey an essentially normal distribution with fixed standard deviation. It is then justified to assume that the next event with clear P-phase arrivals comes from the same set of

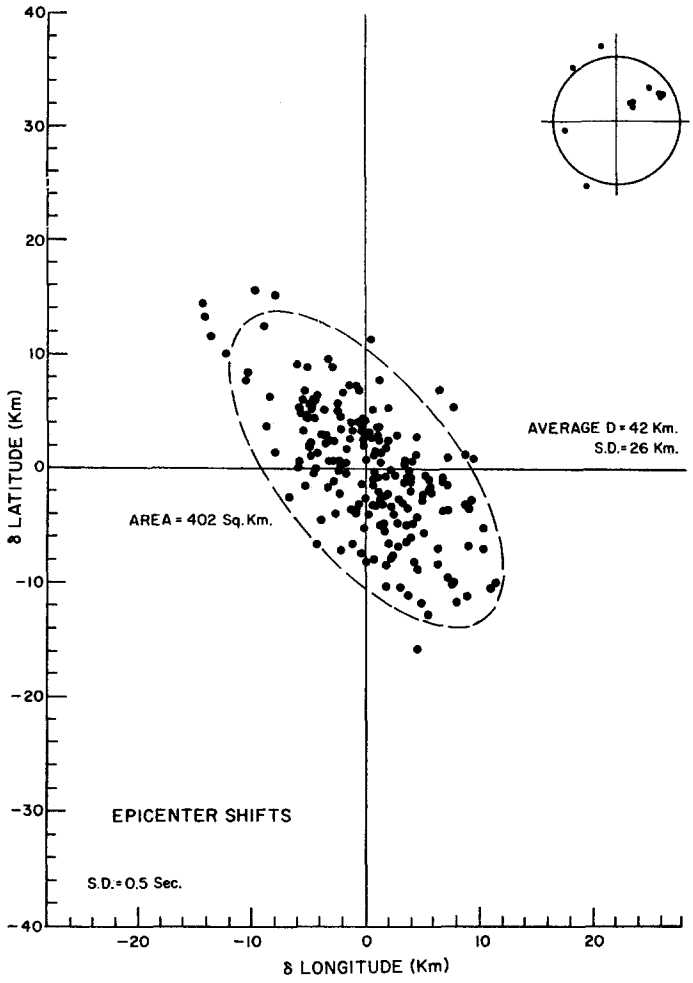

FIG. 20. Epicenter shifts.

travel-time data as all the previously studied events. Again remember that fiducial ellipses are not designed to handle systematic departure of observed travel times from the travel-time curve being used. They are no more capable of doing this then are χ_2^2 or coverage ellipses. The mere fact that they are larger does not mean that they more meaningfully handle the problem. Therefore, it seems that an estimate of the standard deviation of the data of a single event is legitimately obtained from the past history of seismological observation and that it is not required to estimate this value from the data of each event as it occurs. The use of χ_2^2 coverage ellipses is then justified if valid estimates of standard deviation of the data being used have been made.

Figures 24–32 present an evaluation of the detection and location capabilities of a worldwide net of seismograph stations composed of 44 worldwide standard seismograph (WWSS) stations. The stations in the network include all WWSS stations with short-period instrument gains of 25K or greater, Table 8 providing details of location and instrument performance. The technique employed is to develop a computer program which allows statistical evaluation of the detection and location capability of a given

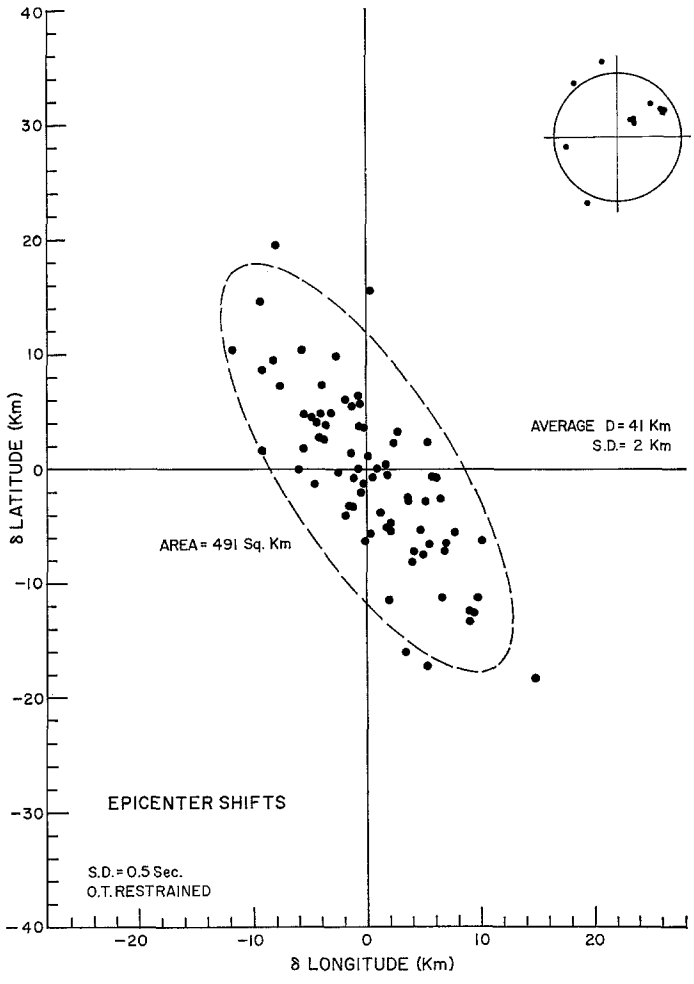

FIG. 21. Epicenter shifts.

network of stations within any area of interest. The program can be applied to both long-period and shlrt-period data. Input data to the program include:

(a) *Station Locations and Noise Levels.* Noise levels are estimated from the operating gains of the short- and long-period instruments at all stations as reported in Handbook of the Worldwide Standard Seismograph Network as revised July, 1966.

(b) *Noise and Signal Variances.* Both variances are assumed to be 0.3 expressed in magnitude units.

(c) *B-Factor Curve.* For short-period body waves, the *B*-factor curve used is that recently developed by J. Clausen. No path correction factors are used.

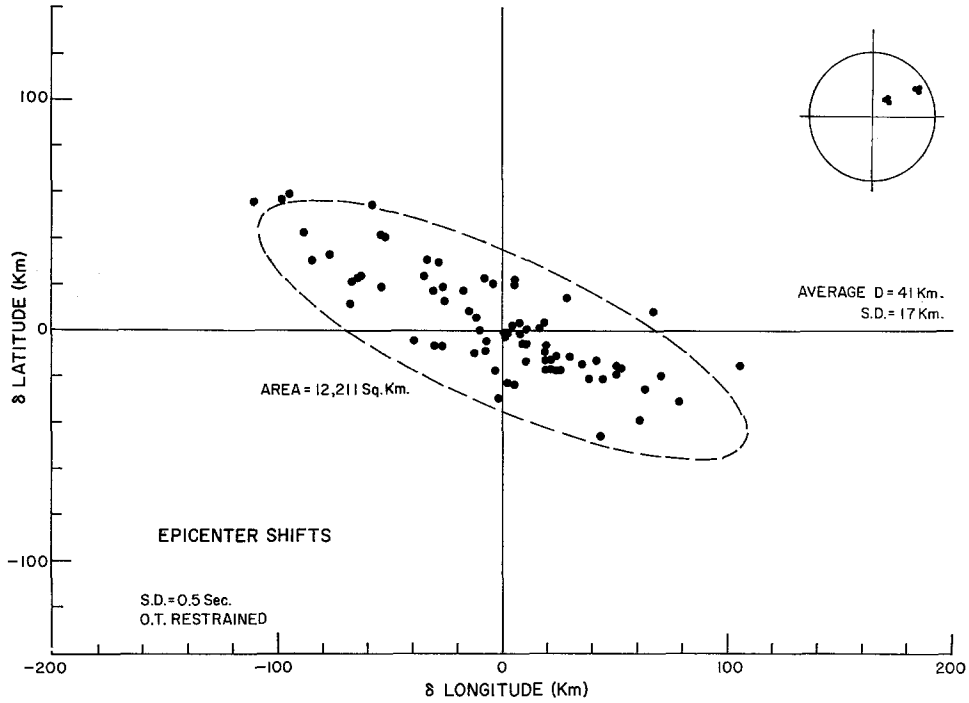

FIG. 22. Epicenter shifts.

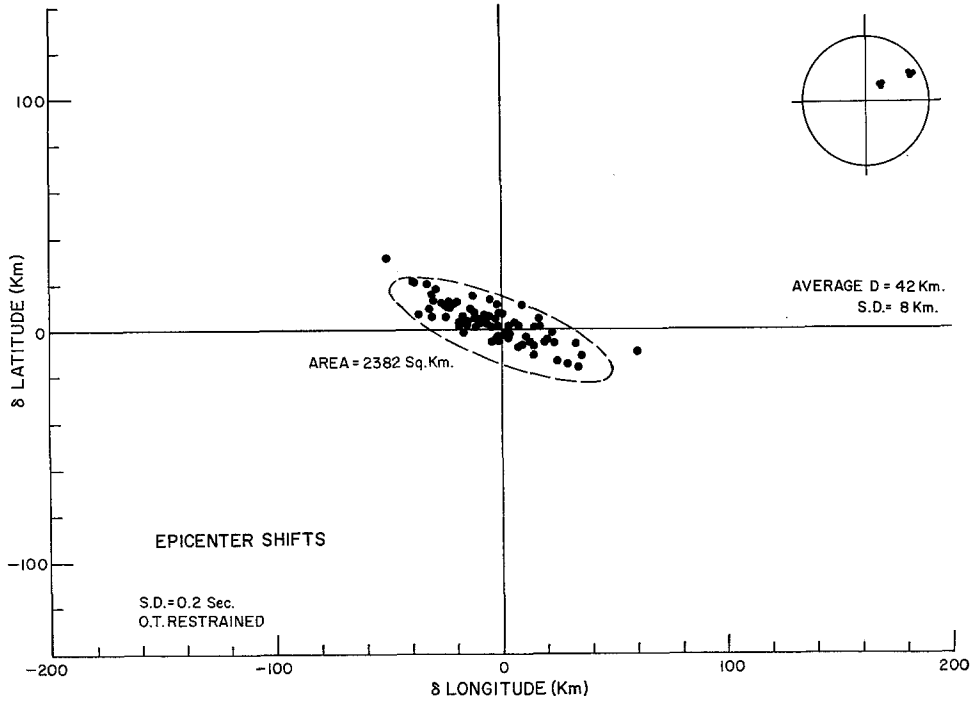

FIG. 23. Epicenter shifts.

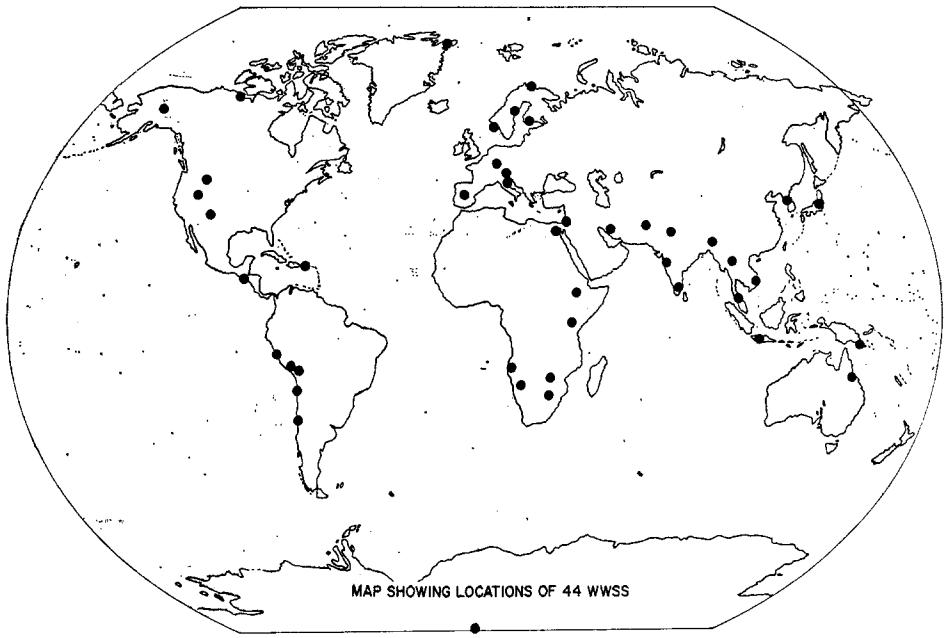

FIG. 24. Map showing locations of 44 WWSS.

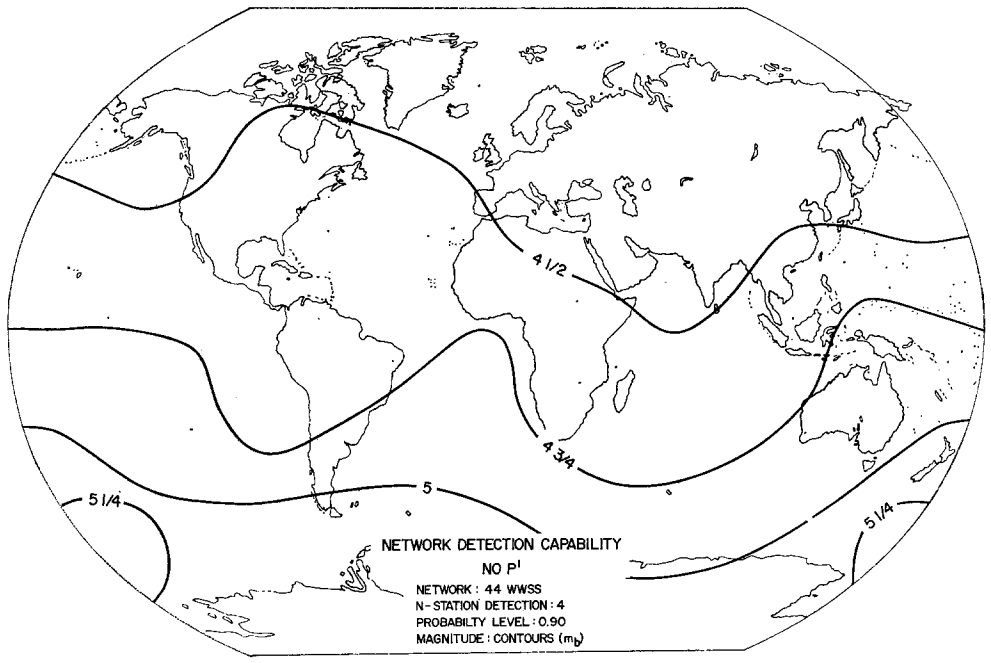

FIG. 25. Network detection capability.

(d) *Signal-to-Noise Ratio Required for Detection.* The signal-to-noise ratio required for detection or accurate phase measurement was assumed to be 1.5. Intensive research supports the correctness of this figure if readings are of LRSM quality or better.

(e) *Station Detection Level Required at Assigned Probability.* At least 4-station detection at 0.90 probability level is required on all maps.

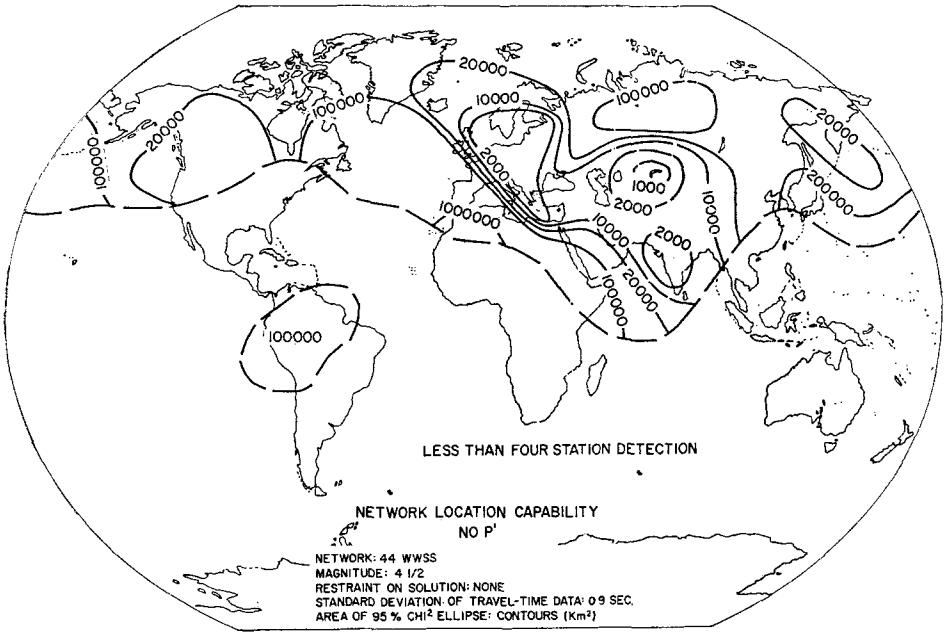

FIG. 26. Network detection capability.

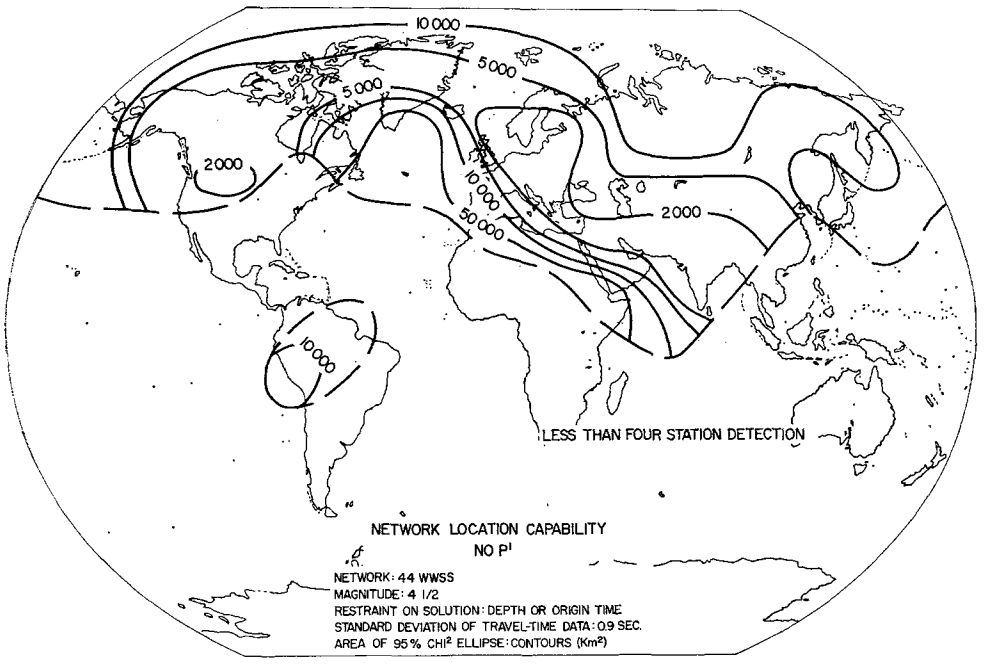

FIG. 27. Network detection capability.

(f) *Network of Test Epicenters.* A sufficient number of worldwise test epicenters (118) were used to allow valid contouring.

(g) *Standard Deviation of Travel-Time Data.* It is assumed to be 0.9 seconds for stations of WWSS quality. (See discussion of this point in the Introduction.)

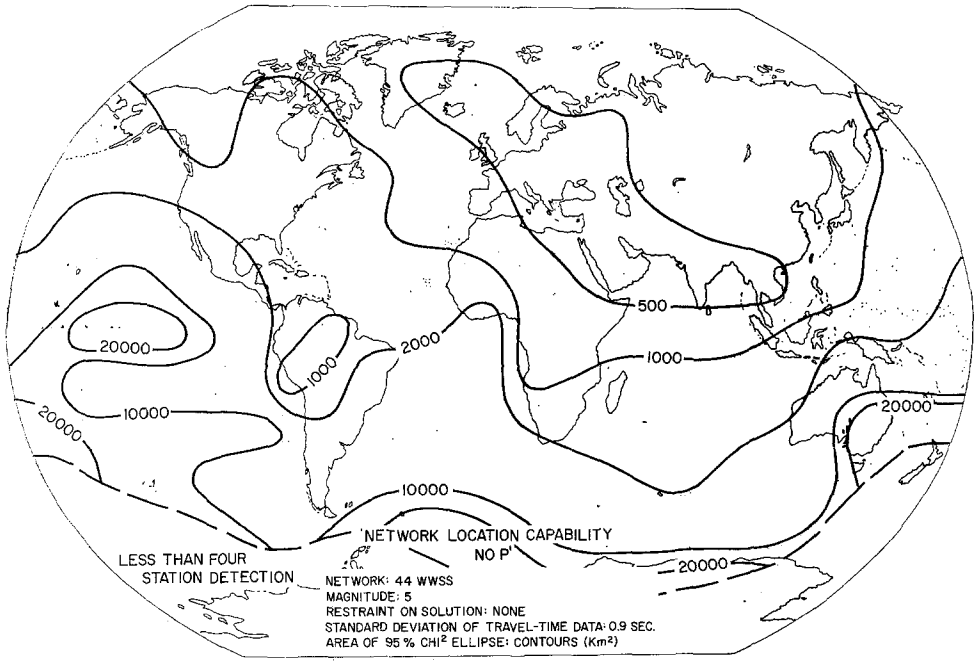

FIG. 28. Network detection capability.

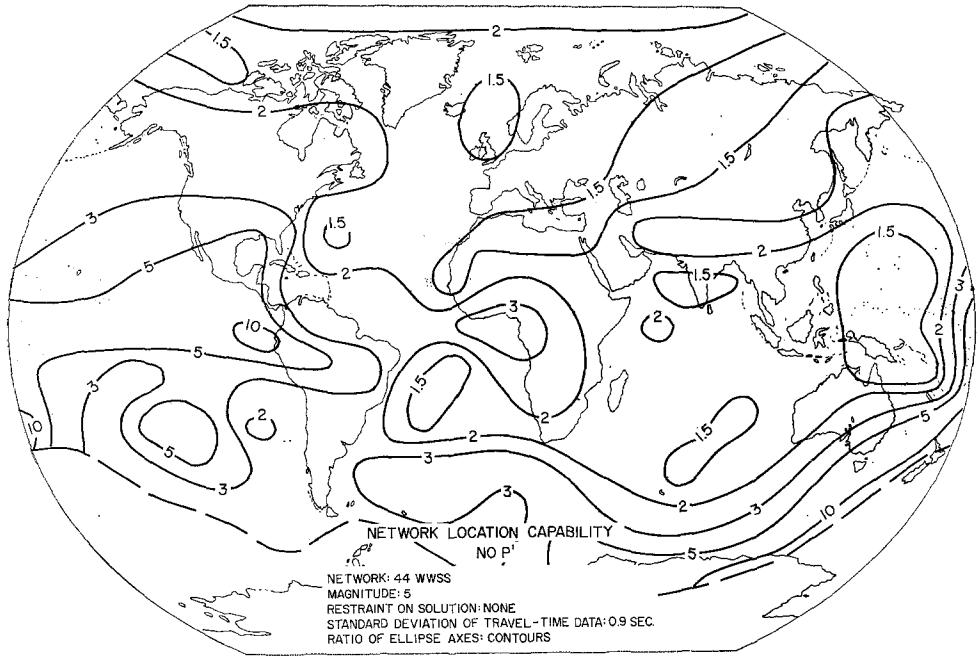

FIG. 29. Network detection capability.

The procedure in the program is, for a given test epicenter, to

(a) Compute distance of all stations,

(b) Compute expected amplitude of each signal at each station as a function of magnitude.

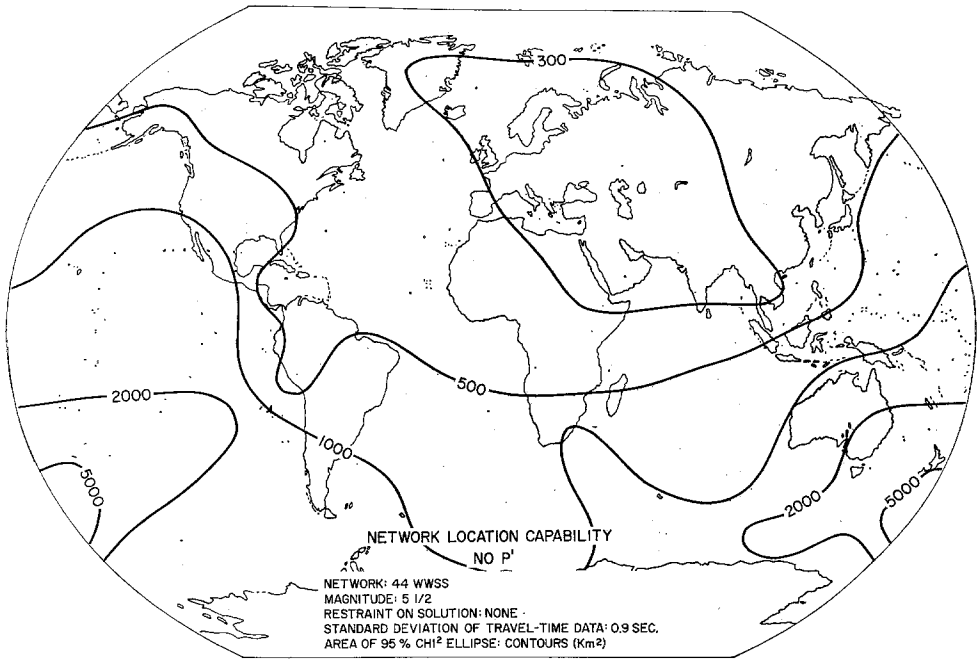

FIG. 30. Network detection capability.

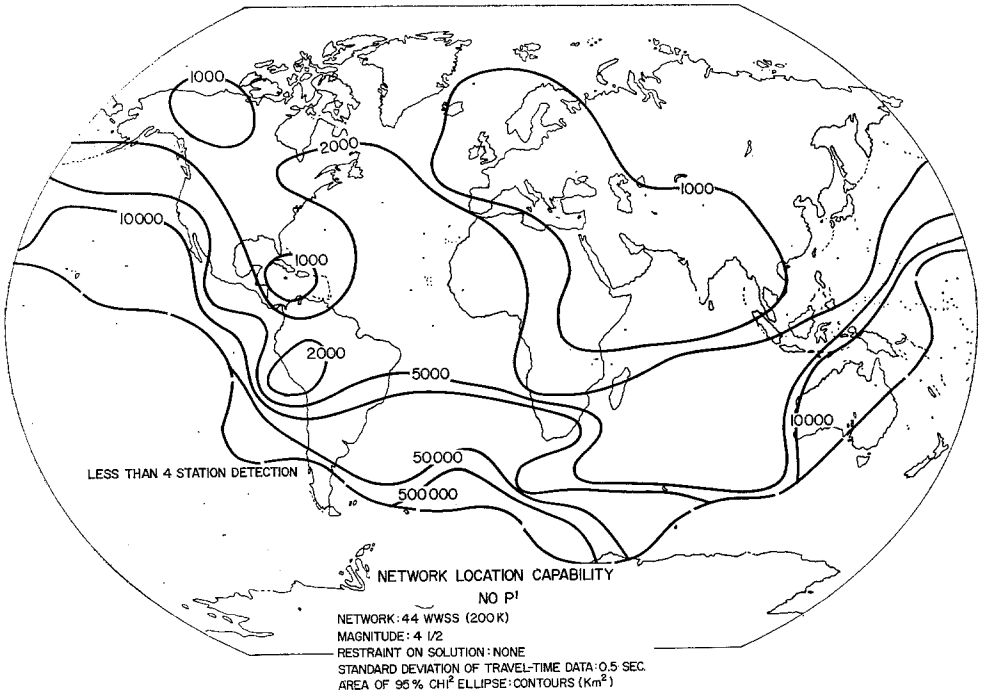

FIG. 31. Network detection capability.

(c) Compare this expected amplitude of signal with station noise level and compute probability of detection at each station as a function of magnitude.

(d) With the set of individual station probabilities, compute the magnitude at which the network has at least an 0.90 probability of 4-station detection (Figure 25, for example), or

(d′) Compute the N-station detection level at 0.90 probability as a function of magnitude.

(e) At magnitudes of interest, select the N most probable detecting stations (N having been established under d') and compute the area of the 0.95 probability χ^2

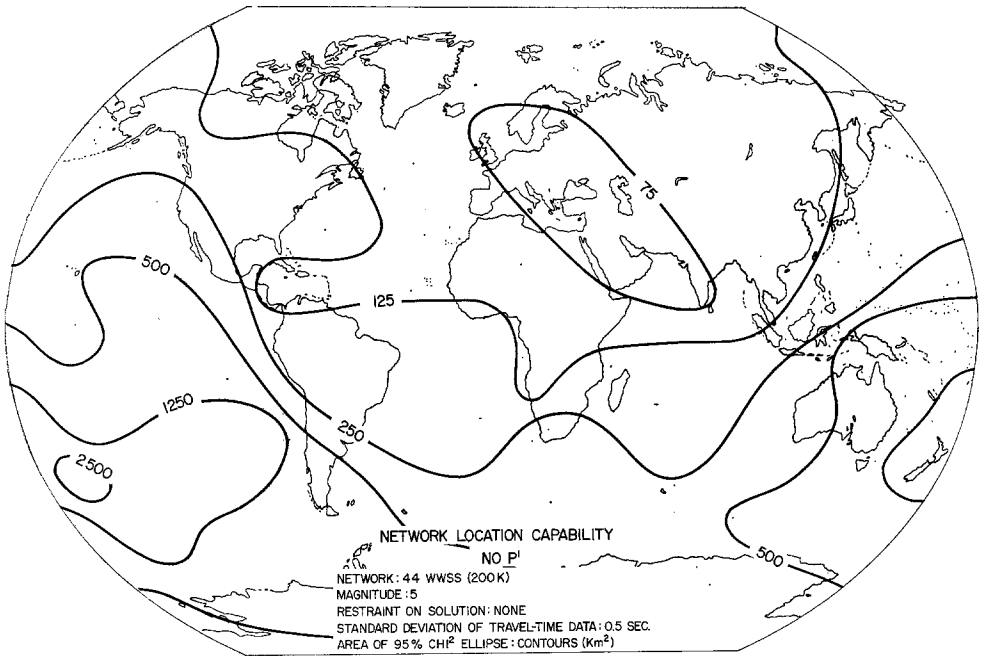

FIG. 32. Network detection capability.

ellipses based on these stations (Figures 26–32). Axial ratios of these ellipses can be contoured as in Figure 29.

Noise level as used here is the mean maximum noise level in the 0.5–3 cps passband. RMS noise in the passband is about $\frac{1}{3}$ of the mean maximum noise. Gains of WWSS stations as listed in the WWSS Handbook are converted to equivalent noise level by comparison with data of stations for which both gain and noise level are known. Estimates of network capability here given presume a quality of record, timing, and interpretation not now attainable at many of the stations. All figures of this report are to be interpreted in terms of network capability at the indicated magnitude. Thus, in the current terminology, these maps are expressive of incremental capability rather than of cumulative capability.

Such figures as Figure 25 actually have little use in evaluating network location capability as no measure of azimuthal distribution of the detecting stations is incorporated in the contoured parameter. A measure of location capability is obtained by computing the expected size and shape of location error ellipses as a function of mag-

TABLE 8

44 WWSS STATIONS

No.	Station	Latitude	Longitude	Short-Period Noise Level	Long-Period Noise Level	Sigma
1	DUG	40.20 N	112.80 W	2.50	550	.20
2	CHG	18.80 N	99.00 E	2.50	550	.20
3	BOZ	45.60 N	111.60 W	2.50	700	.20
4	ALQ	34.90 N	106.50 W	2.50	550	.20
5	CMC	67.80 N	115.10 W	5.00	550	.35
6	KOD	10.20 N	77.50 E	5.00	1100	.35
7	QUE	30.20 N	66.90 E	5.00	550	.35
8	SHL	25.60 N	91.90 E	5.00	550	.35
9	AQU	42.30 N	13.40 E	10.00	550	.40
10	BUL	20.10 S	28.60 E	10.00	1100	.40
11	COL	64.90 N	147.80 W	10.00	1100	.40
12	CTA	20.10 S	146.20 E	10.00	550	.40
13	LPS	14.30 N	89.20 W	10.00	1100	.40
14	MAT	36.50 N	138.20 E	10.00	275	.40
15	SDB	14.90 S	13.60 E	10.00	1100	.40
16	SHI	29.60 N	52.90 E	10.00	1100	.40
17	SPA	90.00 S	0	10.00	4150	.40
18	WIN	22.60 S	17.10 W	10.00	550	.40
19	AAE	9.00 N	38.80 E	20.00	1100	.40
20	ANT	23.70 S	70.40 W	20.00	550	.40
21	ARE	16.40 S	71.50 W	20.00	550	.40
22	HLW	29.90 N	31.30 E	20.00	550	.40
23	JER	31.80 N	35.20 E	20.00	1100	.40
24	KON	59.60 N	9.60 W	20.00	1100	.40
25	LPB	16.50 S	68.10 W	20.00	1100	.40
26	NAI	1.20 S	36.80 E	20.00	1100	.40
27	NDI	28.70 N	77.20 E	20.00	1100	.40
28	NHA	12.20 N	109.20 E	20.00	1100	.40
29	NNA	12.00 S	76.80 W	20.00	275	.40
30	NOR	81.60 N	16.70 W	20.00	2170	.40
31	PEL	33.10 S	70.70 W	20.00	1100	.40
32	PMG	9.40 S	147.20 E	20.00	550	.40
33	POO	18.50 N	73.90 E	20.00	550	.40
34	PRE	25.70 S	28.20 E	20.00	1100	.40
35	SEO	37.70 N	127.00 E	20.00	2170	.40
36	SJG	18.10 N	66.10 W	20.00	2170	.40
37	SNG	7.20 N	100.60 E	20.00	550	.40
38	TOL	39.90 N	4.90 W	20.00	1100	.40
39	TRS	45.60 N	13.80 E	20.00	1100	.40
40	UME	63.80 N	20.20 E	20.00	1100	.40
41	STU	48.80 N	9.30 E	40.00	2170	.40
42	NUR	60.50 N	24.60 E	40.00	1100	.40
43	KEV	69.70 N	27.00 E	40.00	1100	.40
44	LEM	6.80 S	107.60 E	40.00	2170	.40

nitude and stations detecting. Figures 26, 27, and 28 are of this type. It is extremely important to remember that the travel-time errors are assumed to be random in these calculations. If systematic errors are present in the data (i.e., if the travel-time curve used is not expressive of the actual earth conditions), errors in location will result which may be far larger than predicted by these ellipse calculations. Figures 26–32 illustrate clearly the varying capability of a network as a function of epicentral location and

detecting station distribution and are much more useful than the N-station detection figures in evaluating details of network performance. Figure 29 is complimentary to Figure 28 and indicates axial ratios of the error ellipses. High eccentricity is related to poor azimuthal distribution of detecting stations. Figures 31 and 32 indicate the improvement in network location capability resulting if all WWSS stations were improved to 200K stations. Such stations would still be more than an order of magnitude less capable than TFSO.

Location capability of the 44 WWSS network is essentially non-existent at magnitude $4\frac{1}{2}$ and below throughout the World. At magnitude 5, this network is highly useful throughout Eurasia, Africa, South America, and North America, remaining inadequate throughout most of the Pacific and Antarctica. At magnitude $5\frac{1}{2}$, it has adequate capability throughout most of the world. It would be a useful network at magnitude $4\frac{1}{2}$ throughout most land areas of the world if many of its stations were improved to 200K gains.

References

Evernden, J. F. (1969). Identification of earthquakes and explosions by use of teleseismic data, *J. Geophy. Res.*, in press.

Flinn, E. A. (1965). Confidence regions and error determinations for seismic event location, *Review of Geophysics* **3**, 157–185.

Herrin, E., *et al.* (1968). 1968 Seismological tables for *P* phases, *Bull. Seism. Soc. Am.*, **58**, 1193–1228.

Advanced Research Projects Agency
Washington, D. C. 20301

Manuscript received November 19, 1968.